ORGANISMAL BIOLOGY

Muscle-controlled physics simulations of bird locomotion resolve the grounded running paradox

Pasha A. van Bijlert[1,2]*, A. J. "Knoek" van Soest[3], Anne S. Schulp[1,2], Karl T. Bates[4]

Humans and birds use very different running styles. Unlike humans, birds adopt "grounded running" at intermediate speeds—a running gait where at least one foot always maintains ground contact. Avian grounded running is a paradox: Animals usually minimize locomotor energy expenditure, but birds prefer grounded running despite incurring higher energy costs. Using predictive gait simulations of the emu (*Dromaius novaehollandiae*), we resolve this paradox by demonstrating that grounded running represents an optimal gait for birds, from both energetics and muscle excitations perspectives. Our virtual experiments decoupled effects of posture and tendon elasticity, biomechanically relevant anatomical features that cannot be isolated in real birds. The avian body plan prevents (near) vertical leg postures, making the running style used by humans impossible. Under this anatomical constraint, grounded running is optimal if the muscles produce the highest forces in crouched postures, as is true in most birds. Shared anatomical features suggest that, as a behavior, avian grounded running first evolved within non-avian dinosaurs.

INTRODUCTION

Understanding why animals move in certain ways is a fundamental goal of biomechanics, ecology, and evolutionary biology. It is reasonable to assume that animals evolve functional compromises between different features beneficial to their survival (*1*). In terrestrial vertebrates, many factors have been suggested to affect gait selection, including (minimization of) energy expenditure (*2–6*), center of mass (COM) movements (*7*, *8*), neuromuscular factors (*9–11*), gross morphology (*12*, *13*), injury prevention (*14*), and musculoskeletal stresses (*15–18*). By nature, some of these represent conflicting demands, and understanding which factors are dominant in an organism can shed light on what selective pressures may have shaped its evolutionary history.

With such fundamental trade-offs in mind, bipedal walking and running (striding) gaits present some clear mechanical challenges: Life on two legs is less stable than on four, and mass-specific forces on the limbs are roughly twice as high [e.g., (*7*)]. Despite these apparent challenges, large ratite birds are notable for their ability to reach speeds up to 14 to 17 m s^{-1} (50 to 60 km hour^{-1}) (*19–23*), and both ratites and humans are capable of economical locomotion (*3*, *6*). It has been well established that animals prefer different gaits depending on the desired speed, which contributes to minimization of the metabolic cost of transport (MCOT; in joules per kilogram per meter) (*2*, *5*, *6*). Whether animals achieve this by deliberately minimizing muscular work is a matter of debate—among other accountings, low MCOT has been argued to be the result of avoiding activating large fractions of muscle quickly (*4*), the result of avoiding peak muscle activations [thought to represent fatigue avoidance (*11*, *24*)], and a byproduct of avoiding high musculoskeletal forces (*16*). Furthermore, modeling studies have shown that combinations of

work and activation- or excitation-costs [henceforth referred to as "fatigue" following (*24*)] can result in similar gaits (*25*).

In bipeds, the forward speed of the COM is minimal near midstance, regardless of the gait. The vertical position of the COM at this instant is gait dependent: When walking, the COM is at its highest near midstance, whereas when running, the COM is at its lowest near midstance (Fig. 1A). This observation can be described in energetic terms: Walking is a pendular (vaulting) gait, where kinetic (E_K) and potential energies (E_P) of the COM are out of phase (*1*, *7*, *8*, *13*, *26*, *27*). In contrast, fluctuations in COM energy are in phase during running, resembling a bouncing gait (*1*, *7*, *8*, *13*, *27*).

In humans, the walk-to-run transition is accompanied by an abrupt drop in duty factor (DF; fraction of the stride period that a foot is in contact with the ground) (Fig. 1B) (*28*, *29*). Above the transition speed, humans switch to a running gait with an aerial phase (DF < 0.5). In birds, no such abrupt transition in stride kinematics exists (*5*, *13*, *28–32*). Birds transition from walking to running without a discontinuity in DF (Fig. 1C): They first switch to what has become known as a grounded running gait; that is, a gait with no aerial phase (DF > 0.5) but with in-phase COM oscillations (*5*, *13*, *28*, *30–32*). At higher speeds, DF steadily decreases until aerial running occurs. This means that the absence of an aerial phase is not enough to determine whether birds (and even many quadrupedal animals) are running (Fig. 1C) (*7*).

Grounded running has higher energy costs than aerial running, both at the same speed (*27*) and when the gaits are compared at different speeds (*5*, *6*, *32*). In humans, this is often attributed to the higher net joint moments required in crouched postures (*27*, *33*). Avian preference for grounded running at intermediate speeds is thus paradoxical: They appear to habitually prefer a running style that is energetically costly, whereas most animals usually adopt energetically (near) optimal gaits. This paradox has been the subject of much debate (*5*, *6*, *21*, *28*, *31*, *32*, *34*, *35*). Grounded running decreases accelerations at the head, increases stability, and may aid injury prevention (*27*, *28*, *31*, *33*, *35*). The "walk-to-run" transition in ostriches occurs at a higher speed than the "run-to-walk" transition (*21*). While these aforementioned findings suggest the possibility that energetics are not the most important determinant in avian gait

[1]Department of Earth Sciences, Faculty of Geosciences, Utrecht University, Vening Meinesz Building A, Princetonlaan 8A, 3584 CB Utrecht, Netherlands. [2]Naturalis Biodiversity Center, Darwinweg 2, 2333 CR Leiden, Netherlands. [3]Department of Human Movement Sciences, Faculty of Behavioural and Movement Sciences, Vrije Universiteit Amsterdam, Van der Boechorststraat 7, 1081 BT Amsterdam, Netherlands. [4]Department of Musculoskeletal and Ageing Science, Institute of Life Course & Medical Sciences, University of Liverpool, The William Henry Duncan Building, 6 West Derby Street, Liverpool L7 8TX, UK.

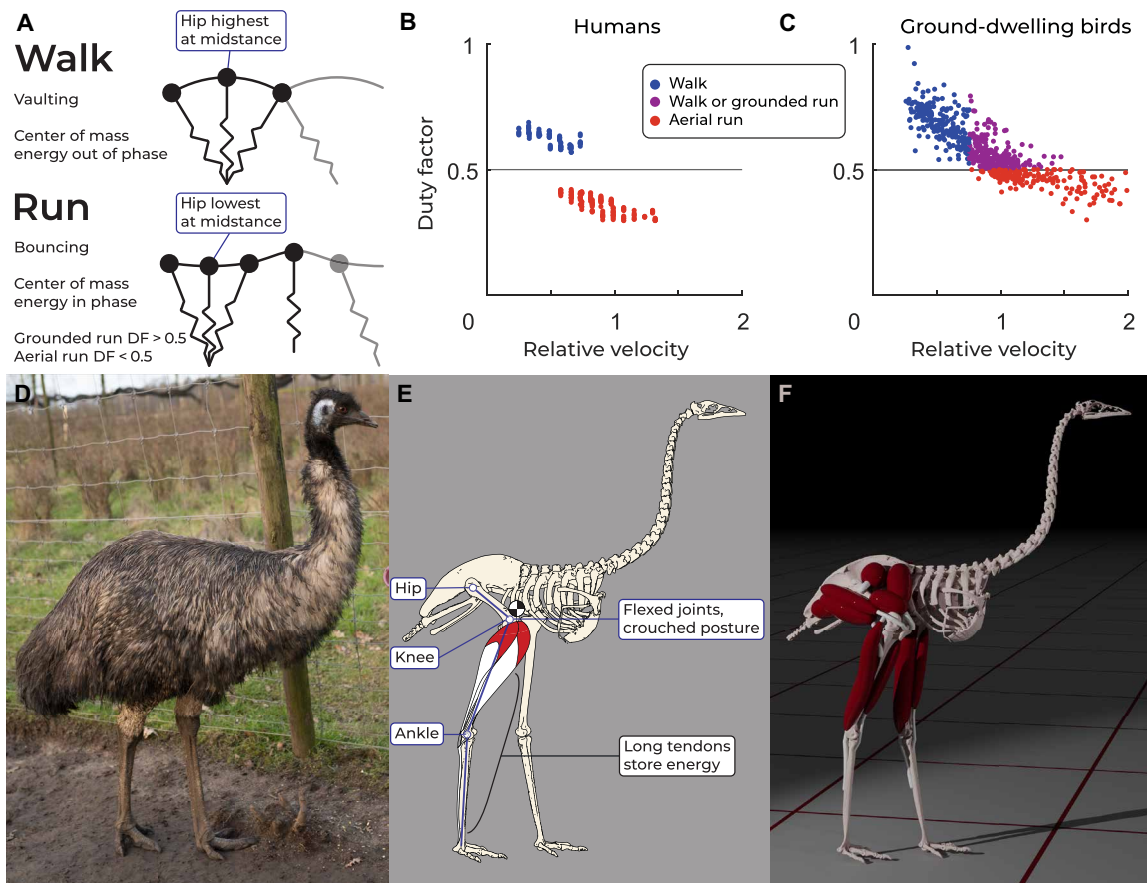*Corresponding author. Email: a.m.vanbijlert@uu.nl, pasha.vanbijlert@naturalis.nl

Fig. 1. Features of walking and running in birds and humans focused on in this study. (**A**) When walking, the hip reaches its highest point during midstance (kinetic and potential energy of the COM are out of phase). When running, the hip reaches its lowest point at midstance (COM energies are in phase). Running gaits are further categorized by duty factor (DF): In grounded running, DF is above 0.5 (and there is, thus, no aerial phase), and in aerial running, DF is below 0.5 (signifying an aerial phase during the gait cycle). DF plotted against relative velocity (dimensionless speed; see Materials and Methods) in (**B**) humans and (**C**) birds. In humans, the walk-to-run transition is marked by a stark reduction in DF. In contrast, birds first smoothly transition to grounded running, and, thus, their gaits cannot be recognized on the basis of DF alone. It is currently unclear why birds prefer grounded running at intermediate speeds. Data plotted in (B) and (C) are modified from Bishop *et al.* (*29*). (**D**) In the emu (*D. novaehollandiae*), as in most birds, the hip and knee joints are enveloped in feathers, obscuring the fact that (**E**) most birds habitually keep their three functional leg segments in crouched postures because their muscles are strongest near these postures. Grounded running in birds may be related to these crouched postures, and/or the presence of extraordinarily long tendons in the distal hindlimb, which enable elastic energy storage. A fully extended posture is impossible for birds due to the forward placement of the COM (checkered circle). (**F**) Our musculoskeletal model of the emu, developed for this study, enabled us to decouple the effects of posture and tendon elastic storage on running gaits.

selection, this seemingly contradicts studies that show that birds do minimize MCOT during gait selection (*5*, *6*). Alternatively, there may be anatomical reasons why grounded running is metabolically optimal for birds but is suboptimal in humans.

One possible anatomical reason for the avian preference for grounded running is elastic energy storage in tendons (*5*, *21*, *31*). Locomotor adaptations in large ratite birds are well established: They have very long digital flexor tendons that store energy when the toes are extended (Fig. 1E) (*19*, *20*, *36*–*38*), and similar mechanisms have been demonstrated in much smaller birds as well (*9*, *39*). It has been estimated that elastic energy storage is more than twice as high in ostriches as in humans (*38*), representing an important factor in avian gait selection.

Another important anatomical feature related to grounded running is the habitually crouched (i.e., flexed) postures that birds adopt (*13*, *28*–*30*, *40*) (Fig. 1, D and E). Small- to mid-sized animals tend to adopt joint poses close to which their muscles can generate the highest forces (*10*), and tendon elasticity in birds biases them toward more crouched postures (*41*). Humans are an exception in this regard, preferring a fully extended, columnar posture (*40*), although they are strongest in crouched postures (*42*). Such a fully extended posture is impossible for birds because their COM lies in front of the hip joint, requiring crouched postures to maintain balance (*40*, *43*, *44*) (Figs. 1E and 2B). Crouched postures appear to be a prerequisite for grounded running in humans (*27*, *33*). Although such a relationship has not been established in birds, recent work modeling bird locomotion as a simple spring-loaded inverted pendulum (SLIP) (Fig. 1A) suggests that grounded running requires sufficient spring compliance (*34*). The SLIP model reduces the hindlimb to a rigid rod mounted on a compliant spring. Unfortunately, there is no clear correspondence between changes in SLIP model leg length and joint poses in the animals modeled in (*34*), and the compliance (or stiffness) of the whole leg
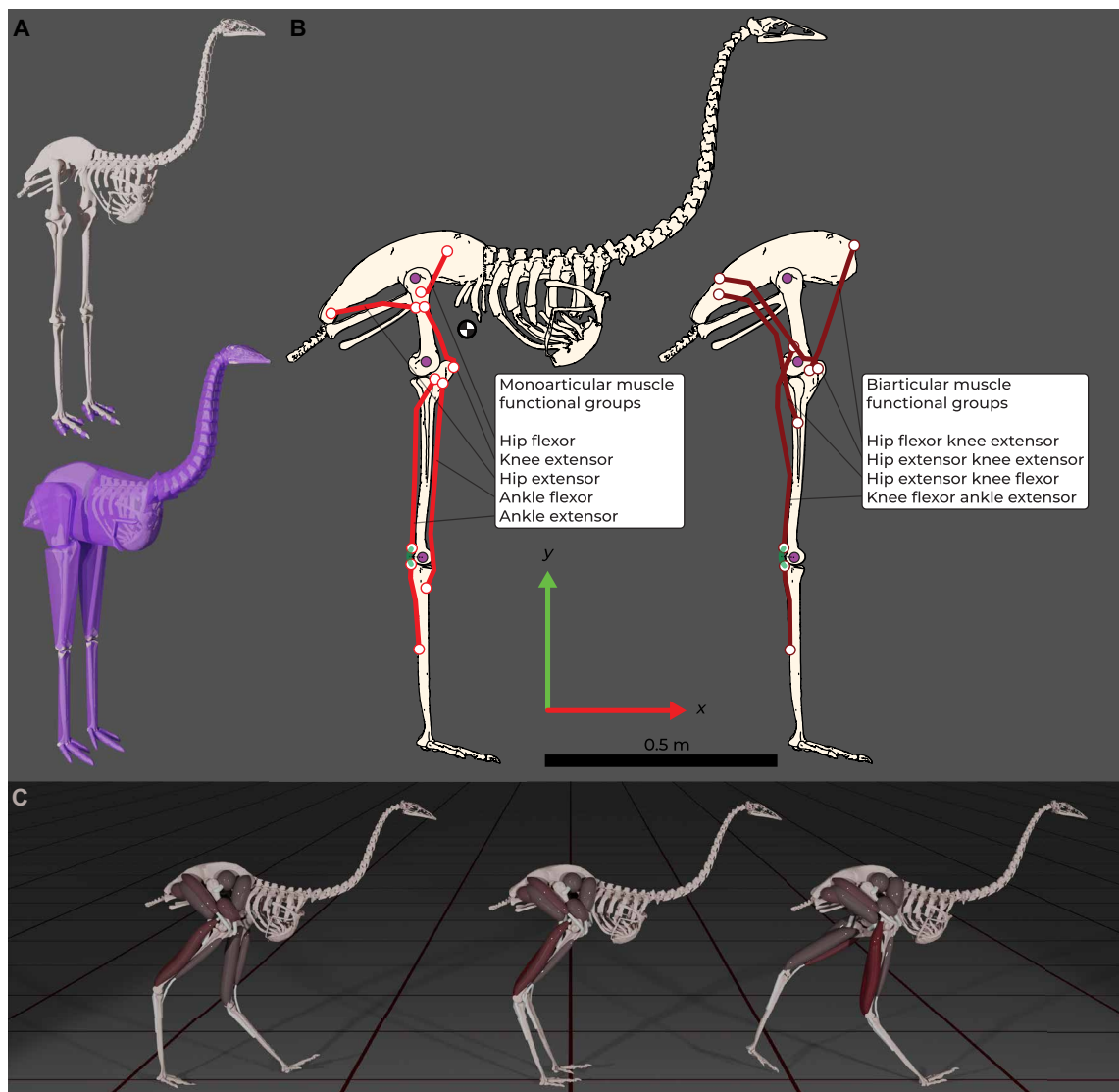
Fig. 2. Overview of methodological steps from model construction to dynamic simulation. (**A**) Top: Symmetrized skeletal model derived from computed tomography (CT) scans, positioned in a neutral reference pose. The model has 10 contact spheres per foot. Bottom: Skin outlines for the model based on convex-hull reconstructions. (**B**) Orthographic projection of the joint centers and paths (lines of action) of the muscle functional groups. Ankle extensors have wrapping cylinders of 0.03 m in radius (in green). We assume a right-handed reference frame. (**C**) Muscle-controlled dynamic simulation, generated de novo without using measured emu kinematics.

cannot always be related to compliance at the level of the individual joints (*45*). It is also unclear whether energy storage in the SLIP model spring has a biological interpretation because "spring-like" leg actuation can be optimal in conceptual models that use telescopic leg actuators (in the absence of any springs) (*25, 46, 47*). Thus, the relative contributions of posture and elastic storage, and therefore the mechanistic triggers for habitual grounded running in birds, remain poorly understood.

Decoupling the mechanical effects of tendon elasticity and crouched postural tunings in a bird in vivo is impractical (if not impossible) and would raise ethical concerns. Furthermore, birds are not easily trained to adopt different running styles at the same speed, further preventing direct comparisons of different gaits (*5, 32*). Instead, musculoskeletal modeling represents an ideal vehicle to test such a phenomenon. Multibody dynamic analysis using such models

has been used in both human (*24, 48–53*) and comparative (*41, 43, 54–59*) contexts and can provide insights complementary to physical experiments (*13*). When such models are combined with optimal control methods [e.g., (*48, 60*)], gaits can be found without using kinematic (motion capture) data as an input, often referred to as "predictive simulation." Predictive simulation is particularly attractive for the present study: It enables us to investigate how (altered) musculoskeletal design affects gait selection, without a priori biasing the model toward desired (measured) gaits. Such insights would not be possible through experimentation but require that ample data exist to validate simulator outputs. The emu (*Dromaius novaehollandiae*) is a large, flightless bird native to Australia (Fig. 1D) (*23, 61*). Although little is known about their locomotor behaviors in the wild, emu locomotion and anatomy are well studied (*6, 17, 20, 22, 28–30, 37, 54, 55, 62–64*), making emus a suitable

model organism for locomotor research. Emus are known to adopt grounded running at intermediate speeds (*17*). In this study, we constructed a new three-dimensional (3D) musculoskeletal model of the emu for predictive multibody dynamic gait simulations (Figs. 1F and 2). This model enabled us to relate musculotendon architecture to the optimality of grounded running over a narrow range of speeds [as observed in the larger ostrich (*5*)] versus a wide range of speeds [as observed in much smaller birds (*31*, *32*, *45*)].

Our primary goal was to investigate the grounded running paradox: Why do birds adopt grounded running gaits at intermediate speeds (Fig. 1C), even though studies show (*27*, *32*) that this is energetically costly? We hypothesized that grounded running is an attractive running style for birds because their muscles function optimally in crouched postures, and fully extended (human-like) postures are impossible because of their anatomy. Because grounded running is often referred to as a "compliant gait" with spring-like leg behavior, a secondary goal was to investigate whether grounded running requires any compliance (i.e., any elastic energy storage). We simulated gait transitions in model variants that were tuned to generate peak muscle forces at different postures (columnar, intermediate, and crouched), with both elastic and rigid tendons (Fig. 3). Our simulations provided strong support for our overarching hypothesis and revealed a fundamental trade-off in gait selection. Even when using rigid tendons, our musculoskeletal model was capable of grounded running, bolstering predictions from conceptual models with telescoping limb actuators (*46*, *47*). Thus, we found that grounded running is purely an effect of

changes in effective leg length—no energy storage (or leg spring compliance) is required, it is an effect of limb posture. Grounded running requires crouched postures to achieve (*27*, *28*, *34*). These crouched postures result in higher muscle forces (and thus higher energy costs and fatigue) when compared to columnar postures. However, grounded running results in lower peak ground reaction forces (GRFs), which decreases energy costs (*4*, *65*). There is, thus, a trade-off between minimizing peak muscle forces (columnar postures) and minimizing peak GRFs (crouched postures and grounded running), and humans adopt the former. In contrast, our results demonstrate that grounded running represents a metabolically optimal gait at intermediate speeds for crouched bipeds (such as birds). Grounded running is also optimal from a fatigue (muscle activation or excitation) perspective in our simulations. A columnar, human-like running style could have lower energy costs and fatigue for birds, but this is impossible because of the forward placement of their COM, combined with muscles that generate the most force in crouched postures. As a result, grounded running is energetically optimal at intermediate speeds. Thus, we argue that the paradox in avian gait selection does not exist and that secondary benefits of grounded running in birds are not at odds with the well-established principle of MCOT minimization.

RESULTS

Our analysis relied on systematically tuning the muscular anatomy of the model to generate peak forces in different postures. We
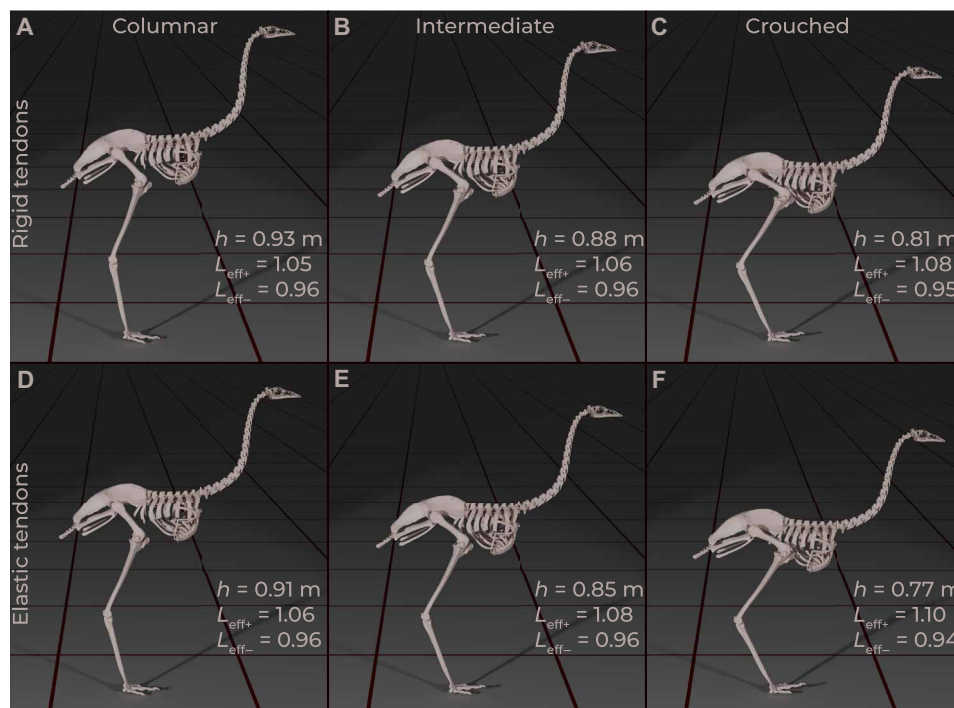

Fig. 3. Midstance poses adopted by all the model variants when walking at 1.25 m s^{-1}. By modifying the musculotendon parameters, we systematically varied the postures at which the muscles generated peak forces. We refer to this as postural tuning. The optimizer was free to select the optimal gaits (and postures) using the changed anatomical parameters, these different postures were thus not explicitly prescribed. The top row depicts midstance poses of rigid tendon model variants tuned for (**A**) columnar, (**B**) intermediate, and (**C**) crouched postures. The bottom row shows midstance poses of elastic tendon model variants, tuned for (**D**) columnar, (**E**) intermediate, and (**F**) crouched postures. Each elastic tendon variant adopted slightly more crouched postures than its rigid tendon counterpart, signified by hip height h. Across the walk-to-run transition, variations in effective leg length (L_{eff+} and L_{eff-}; see Materials and Methods) increased, both with increasingly crouched postures and with elastic tendons.

simulated how the resulting postural bias influenced running styles found through optimization. The variation in postures and running styles was thus achieved by varying the musculotendon parameters, not by explicitly modifying the control parameters for the gaits. We hypothesized that grounded running is optimal for bipeds with crouched habitual postures (such as birds) and not necessarily dependent on elastic storage in tendons. To demonstrate this, our simulations decoupled the effects of leg postural tuning and tendon elasticity. Grounded running occurred more often in our model variants if they had crouched tunings, using a variety of different optimization approaches and model formulations. Elastic tendons, an important factor in bird anatomy, tended to increase the occurrence of grounded running by affecting leg postures, but elastic storage itself was not required for grounded running.

In the next sections, we will first demonstrate that systematic differences in our model variants resulted in systemically different postures and gaits (Fig. 3 and movie S2), and present general patterns related to these differences. We will compare these model variant gaits to real emu data to demonstrate that all the variants captured the salient features of emu locomotion. After this, we will present results that directly support our hypothesis. Unless otherwise specified, we will present data from optimizations where we minimized both muscle fatigue [as defined in (24)] and energetic cost ("fatigue and MCOT"; see Materials and Methods). Fatigue was parameterized as neural input (excitations cubed) and energy cost as the MCOT. The fatigue-only and MCOT-only optimizations are presented as supplementary data and figures. We analyzed more than 650 trials (excluding local optima and pilot simulations).

General patterns
Our muscle tuning procedure successfully biased the model variants as desired to relatively columnar, intermediate, and crouched postures (compare hip heights h in Fig. 3, left to right). Movie S2 demonstrates the different walking gaits of the model variants. Crouched variants showed a larger range in effective leg length (L_{eff}; see Materials and Methods) during the stance phase than more columnar variants, both in relative and absolute terms (Fig. 3, crouched variants in C and F). All elastic tendon model variants adopted more crouched midstance postures and used a wider joint range during locomotion (resulting in lower h and a larger range in L_{eff}) than the rigid tendon variants (Fig. 3, top row versus bottom row).

Despite not having moveable toes, GRFs of all model variants compared favorably to that of real emus over a large range of speeds and gaits (Fig. 4 and figs. S1 and S2). Figure 4 reports both absolute speeds (v; in meters per second) and relative velocities ($\hat{v}$; dimensionless size-normalized speed; see Materials and Methods). At 1.25 m s^{-1}, the vertical component showed a double hump, distinctive to emus, ostriches, and bipeds in general (13, 29, 55). Irregularities in the GRF can be seen at higher speeds—these are related to sequential loading and unloading of neighboring contact spheres. The rigid intermediate model adopted a gait with high impact transients at running speeds (fig. S2), related to initially loading the caudal-most contact sphere (similar to a human heel strike). Overall, our models appeared to capture the salient speed-dependent features of emu locomotion.

DF (relative ground contact time) was consistently higher in crouched model variants, than in their columnar counterparts (Figs. 5, A and C, and 6A and figs. S3 and S4). Similarly, DFs were

higher, and stride lengths were longer in the elastic tendon model variants than in the rigid tendon variants (Fig. 5). Together, this suggests that increasingly crouched postures increase ground contact times (DF) and that elastic tendons have an independent effect due to their effect on postures (see also sensitivity analyses 1 and 2 in the "Sensitivity analysis results" section).

Directional hysteresis of DF and $\hat{L}$
We observed a hysteresis depending on whether the starting point of the sequential gait optimizations was at walking speed or maximal running speed (compare walk-to-run with run-to-walk trials; Figs. 5, A and C, and 6A and figs. S3 and S4; movie S3 demonstrates walk-to-run). Thus, we acquired two gaits at each speed, which near the transition speed could be either aerial or grounded running [similar to SLIP model predictions (34)]. When walking (and thus high DF) was the starting point, the models adopted higher DFs across the transition speeds, and vice versa. We plot them separately because some model variants only adopted grounded running in the walk-to-run sequence (see the "Gait transitions and grounded running" section). See Discussion for an elaboration upon this hysteresis effect.

Gait transitions and grounded running
We defined running as a gait where the phase angle of the COM (ϕ_{COM}; in degrees) is less than 10°. Figure 6B shows that our models transitioned from walking to running at $\hat{v} \sim 0.7$ to 1.1. This is slightly higher than subadult emus, which are reported to switch to running at $\hat{v} \sim 0.66$ (6), although transition speeds in that study were determined visually. Transition speeds were similar in the fatigue-only optimizations but were lower in the MCOT-only optimizations (figs. S3 and S4, respectively). In the MCOT-only optimizations, the rigid tendon models did not display predictable gait transitions (resulting in impulsive gaits, multiple stance phases per leg, or never transitioning back to walking at low speeds). The MCOT-only optimizations using rigid tendons were therefore rejected from our analysis (see Discussion).

We defined grounded running as a gait where ϕ_{COM} was less than 10° (i.e., in phase), combined with a DF of 0.5 or higher (see Materials and Methods and Fig. 1). All model variants adopted grounded running (Fig. 6). In Fig. 6, the occurrence of grounded runs increases from the left to right panels (black circles). This suggests that increasingly crouched postures result in grounded running being the optimal gait over a larger range of speeds. Figure 6 also demonstrates an independent effect of elastic tendons (e.g., compare the rigid crouched to the elastic crouched column): The presence of elastic tendons increased the occurrences of grounded running. This pattern was also observable when fatigue was the singular main cost in the optimizations (fig. S3). In the MCOT-only simulations, the crouched model variant adopted grounded running, while the other model variants did not (fig. S4). Together, these results suggest that grounded running is increasingly advantageous with more crouched postural tunings. The addition of elastic tendons results in more crouched midstance postures and larger ranges in L_{eff} (Fig. 3), strengthening this effect (further supported by the simulations of the "wide range" model variant in the "Sensitivity analysis results" section).

Figure 6C shows MCOT, which we used to compare differences in energy costs between model variants. Because of the deliberately narrow tuning ranges of our models, our model underestimates
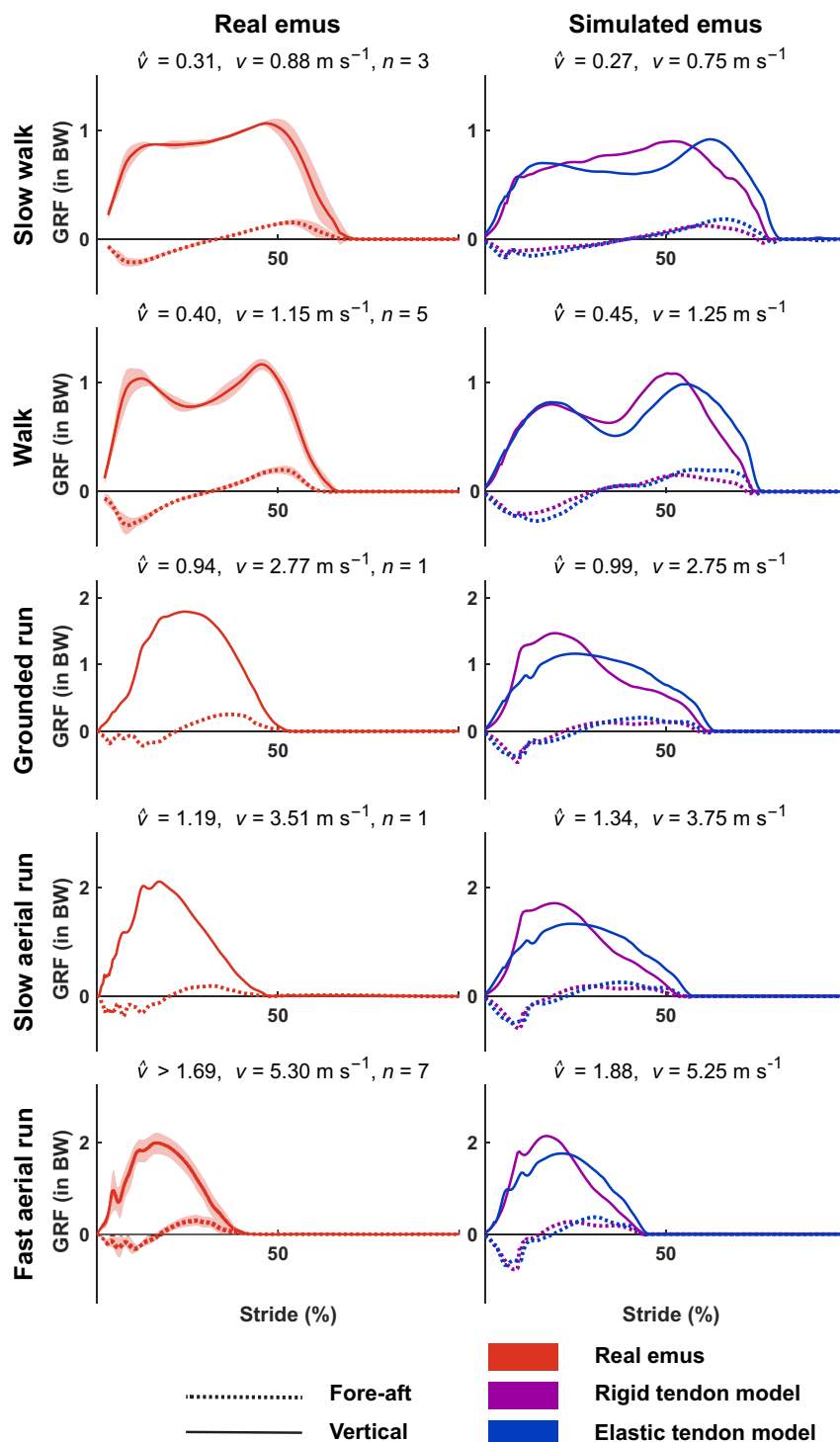
Fig. 4. Ground reaction forces (GRF) of real emus during walking and running compared to our simulations at dynamically similar speeds. GRFs of the real emus (**left**) and our simulations (**right**) are normalized to their respective body weights (BW). We plotted the walk-to-run optimizations of the model tuned for crouched postures (see figs. S1 and S2 for columnar and intermediate postures). Both model variants show the distinctive double hump in the vertical component during walking. Two slow walk trials and all walk trials were provided courtesy of J. Goetz. Grounded and slow aerial run trial and one slow walk trial were provided courtesy of J. Hutchinson. Fast aerial run trials were provided courtesy of R. Main.

MCOT of emus (see the simulations of the "wide range" model variant in the "Sensitivity analysis results" section and the related discussion in the "Limitations" section) (6). Nevertheless, a pattern quite similar to real emus can be observed: a local optimum at low speeds (albeit at a higher speed in our simulations) and then another optimum near 5 m s^{-1} (6). This pattern was less clear in the more crouched model variants, suggesting that these models made less use of pendular energy savings during walking, more akin to the pattern observed in smaller birds (32). Across all simulations, minimum MCOT increased as model variants were tuned for increasingly crouched postures (Fig. 6C and figs. S3 and S4). Figure 3 shows that these model variants adopted increasingly crouched postures across the transition speeds, demonstrating that crouched running styles had higher minimum MCOT in our model. Superficially, this is similar to humans, but unlike McMahon et al. (27), we acquired this result by changing the posture at which the muscles generate the highest forces. Thus, the optimal running postures and minimum MCOT depend on postural tuning in our analysis. This is an important observation: Given that minimal energy cost was one of the explicit optimization goals, this implies that grounded running is an energetic optimum for a crouched biped, despite having an overall higher energetic cost than columnar bipeds.

We also plot our measure of fatigue (the time integral of excitations cubed, normalized, and scaled according to Eq. 2; see Materials and Methods) in Fig. 6D. Increasingly crouched postures required higher muscle activity, resulting in higher fatigue (Fig. 6D). An analogous argumentation to the previous paragraph applies here: Although columnar-tuned bipeds run with lower overall fatigue (Fig. 6D, left), grounded running represents an optimal solution for a crouched biped from a muscle activity perspective.

Together, these results imply that grounded running is an attractive running style for a crouched biped (such as a bird), both from an energetic (MCOT) perspective and from a muscle activation (fatigue) perspective. In our optimizations, relative contributions of fatigue and MCOT were tuned at walking speed (see Materials and Methods). Fatigue increased curvilinearly with speed (Fig. 6D), whereas MCOT did not (Fig. 6C), resulting in an overemphasis on fatigue reduction at higher speeds. In sensitivity analysis 4 (next section), we demonstrate that this does not affect our conclusions.

Sensitivity analysis results

We performed extensive sensitivity analyses to investigate the robustness of our conclusions. This section follows the same order as the "Sensitivity analyses" section in the Materials and Methods.

1) In this sensitivity analysis, we simulated a "no elastic storage" model variant. This model eliminates the possibility that sites of elastic energy storage other than in the tendons facilitated grounded running. We included this because our rigid tendon models could potentially store energy in the ground contacts and muscle fibers [parallel elastic elements (PEEs)] themselves. Our "no elastic storage" model was still capable of grounded running (fig. S5). This demonstrates that grounded running requires no elastic storage (or compliance); it is purely an effect of changes in effective leg length (L_{eff}).

2) In this sensitivity analysis, we simulated an elastic "wide range" model variant. Our main models were deliberately tuned for narrow joint ranges to achieve the different postures and, therefore, may systematically underestimate MCOT (see Materials and Methods). We investigated this effect by simulating a model variant tuned for wide joint ranges. This model adopted grounded running over four different speeds (fig. S6), behaving similar to the elastic crouched model (Fig. 6, rightmost column). Although hip height ($h = 0.84$ m) was closer to our elastic intermediate model (Fig. 3E), the range in effective leg length was much larger ($L_{eff+} = 1.10$ and $L_{eff-} = 0.95$), similar to the elastic crouched model (Fig. 3F). This further emphasizes the significance of L_{eff} when interpreting grounded running. This model had higher MCOT over its entire range (fig. S6), confirming that our narrow tuning ranges resulted in lower MCOT in the main model variants.

3) In this sensitivity analysis, we simulated the "knee flexor" model variants to investigate how the uncertain muscle function of M. femorotibialis medialis might affect gait transitions. We only simulated rigid intermediate and crouched variants (fig. S7). The addition of the knee flexor reduced both overall fatigue and MCOT at higher speeds. The crouched variant still adopted grounded running, but the intermediate variant did not, which is consistent with the interpretation that grounded running is optimal in more crouched tunings.
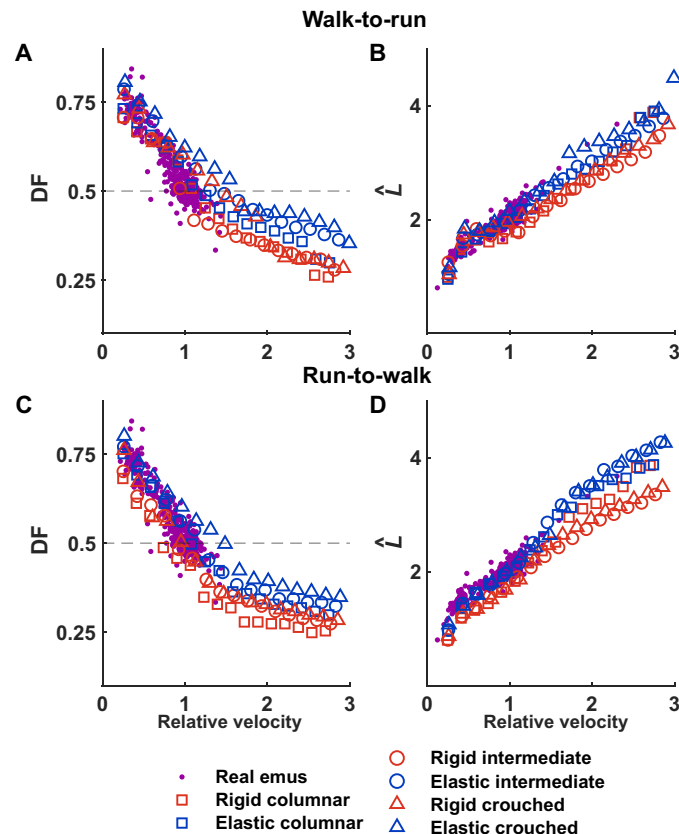

Fig. 5. Duty factors (DF) and relative stride lengths ($\widehat{L}$) adopted by real emus compared to our simulations. We acquired different gaits depending on whether we sequentially increased speed from walking speeds (walk-to-run) (**A** and **B**) or whether we sequentially decreased speeds from the maximal speed (run-to-walk) (**C** and **D**). Rigid tendon models (red) adopted lower DFs and stride lengths than elastic tendon variants (blue). Columnar model variants adopted lower DFs than crouched variants, but this did not (consistently) affect stride lengths. Real emu data are from Gatesy and Biewener (28), Abourachid and Renous (30), Goetz et al. (55), and Bishop et al. (29).
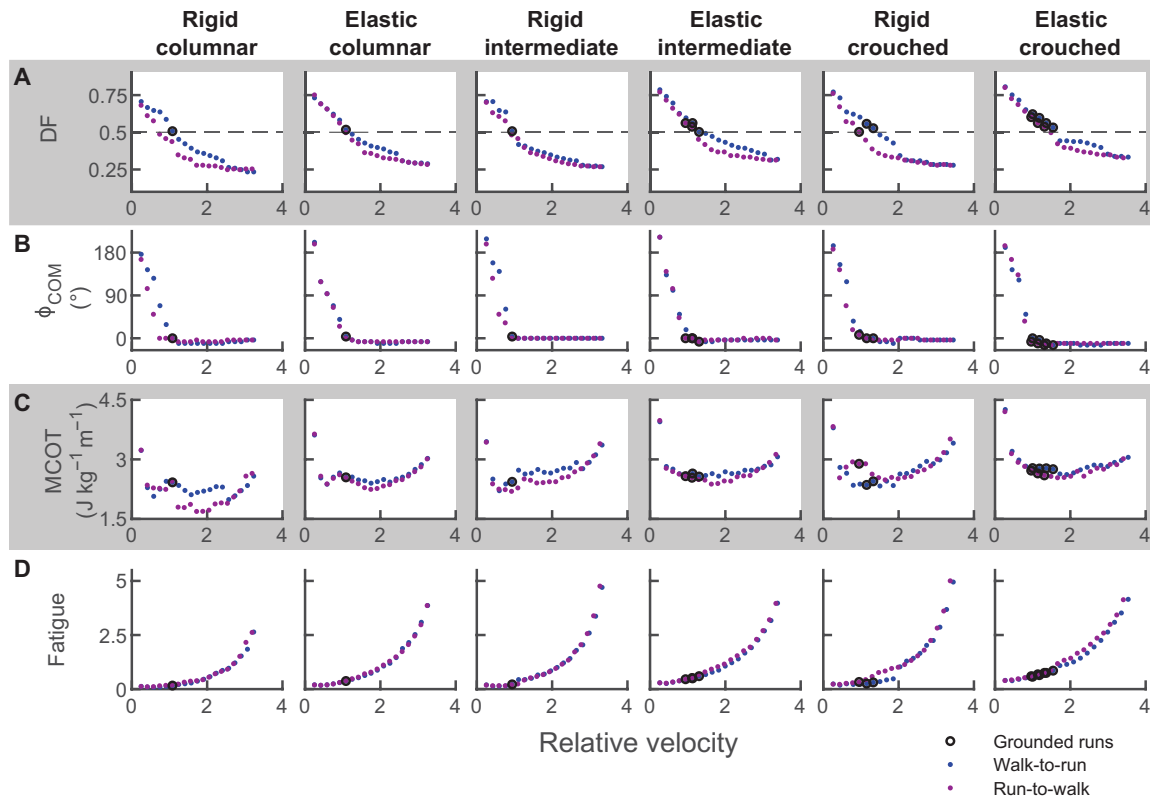
Fig. 6. Gait metrics plotted against locomotor speed, compared between model variants. These converged optimizations used both fatigue and MCOT in the cost function. Each column represents a model variant, with rows from top to bottom showing (**A**) duty factors (DF), (**B**) phase angle of the COM (ϕ_{COM}), (**C**) metabolic cost of transport (MCOT), and (**D**) muscle fatigue. We plot nondimensional relative velocities ($\hat{v}$). In all cases, relative velocities corresponded to a forward velocity range of 0.75 to 9.75 m s^{-1}, but differences in hip height affected relative velocity. Grounded running trials are indicated with black circles. The grounded runs are concentrated toward the right panels in the figure, suggesting that crouched postures increase the occurrence of grounded running. Elastic tendons show an interactive effect, further increasing the occurrence of grounded running. Fatigue is the integral of muscle excitations cubed, normalized, and scaled (see Materials and Methods). Similar to Fig. 5, it can be seen that the models adopted different gaits depending on the optimization direction.

4) In this sensitivity analysis, we reweighted the cost function at 3.25 m s^{-1} to account for possible unforeseen consequences of fatigue increasing disproportionately to MCOT with increasing speeds (Fig. 6, C and D). To achieve equal weighting of fatigue and MCOT at 3.25 m s^{-1}, relative weight of MCOT was increased by a factor of 2.8. Using this rescaled cost function, we ran four more optimizations with a target speed of 3.25 m s^{-1}. For the crouched model, we used two solutions at 9.75 m s^{-1} as the initial guess (DF = 0.33 and 0.23). This still resulted in grounded gaits for the crouched model (DF = 0.53 and 0.52, respectively). These values for DF are lower than in Fig. 6 but demonstrated a tendency for this model to adopt higher DFs. For the columnar model, we reinitialized the optimization using a gait of 9.75 and 2.25 m s^{-1} (DF = 0.23 and 0.62). In both cases, the columnar model switched to aerial gaits (DF = 0.48 and 0.47, respectively). This analysis further bolsters the finding that crouched models tend toward higher DF gaits and grounded running, whereas columnar models do not. It also suggests, similar to the MCOT-only optimizations, that higher weighting of MCOT results in lower DF at the same absolute speed, which would result in the walk-to-run transition to occur at a lower speed.

DISCUSSION

Our main goal was to investigate why birds prefer grounded running at intermediate speeds. We achieved this by decoupling the effects of limb postures and tendon elastic energy storage on simulated gait transitions in the emu, using virtual experiments with a musculoskeletal model. We simulated model variants that were tuned to generate peak muscle forces at different postures (columnar, intermediate, and crouched), with both elastic and rigid tendons (Fig. 3). This approach enabled us to bridge the gap between the mechanical and metabolic explanations for why birds habitually use this gait. We showed that grounded running gaits are possible (and even optimal) in the absence of elastic tendons (Fig. 6 and fig. S5). Thus, elastic energy storage in tendons, an important feature of bird locomotion, is not a requirement for grounded running. Crouched model variants adopted grounded running (and higher DFs in general) over a wider speed range than columnar model variants. This result was acquired regardless of whether the optimization goal was minimal MCOT (fig. S4), muscle fatigue (parameterized on the basis of peak neural input) (fig. S5), or both (Fig. 6). This suggests that the avian tendency toward grounded running is not paradoxical. It is an attractive running style for animals whose muscles function

optimally in crouched postures and is in agreement with well-established MCOT/fatigue minimization strategies (2, 5, 6, 24, 25). Although the evolutionary history of avian leg postures and body shapes is currently still being debated, our simulations support the interpretation that avian grounded running first evolved within non-avian theropods. We will discuss these results and their implications in turn.

Grounded running requires changes in effective leg length, not compliance

Seminal work by McMahon et al. (27) related the angle "made between the thigh and the horizontal at midstance" in running humans to leg compliance, and SLIP models suggest that grounded running requires leg compliance (34). Unfortunately, such a single angle-to-compliance mapping is not generalizable to the three-segment legs of birds (45). More generally, compliance implies energy storage in the spring of SLIP model. This energy storage has no clear physical interpretation, and springless conceptual models with telescopic leg actuators are also capable of grounded running (46, 47). Our simulations demonstrate that energy storage is not a requirement for grounded running (Fig. 6 and fig. S5): The unifying metric is the range in effective leg length during the stance phase.

For fixed joint excursions, the change in effective leg length will be higher at increasingly crouched postures in absolute but especially in relative terms (Fig. 3, compare A to C). This explains why our crouched models more readily lend themselves to grounded running (Fig. 6B). No storage in the abstract "leg spring" is required: It is a by-product of the optimality of a roughly linear relationship between GRFs (or leg forces) and effective leg lengths (25, 46, 47). That is, leg mechanics are "pseudo-elastic"—spring-like leg behavior is energetically optimal even if elastic storage is not possible (46, 47, 66). However, tendon elasticity does shift the joint range at which a muscle produces maximal force (41), which results in more crouched midstance postures and a higher range in effective leg length (Fig. 3, top versus bottom row). Thus, having very compliant or long tendons could still bias a biped with columnar optimal postures to adopt grounded running (e.g., Fig. 6, elastic columnar).

Why is grounded running in birds optimal?

Grounded running is an energetically costlier gait than aerial running (27, 32), yet birds adopt it habitually at intermediate speeds (5, 13, 28, 30). The apparent paradox, given the higher energetic costs associated with these crouched postures, can also be observed in our different model variants, since both MCOT and fatigue increased with more crouched postures (Fig. 6, C and D, and figs. S3 and S4). However, MCOT and fatigue were express costs (to be minimized) during the optimizations. This suggests that grounded running gaits, and higher DF gaits in general, represent (locally) optimal gaits for crouched-tuned bipeds from a muscle energetics and fatigue perspective (Figs. 5, A and C, and 6). Crouched models converged to higher DF gaits than the columnar models, even if extremely fast aerial running was the initial guess (sensitivity analysis 4), further supporting this interpretation. Overall, our analysis demonstrates two competing strategies for energy savings in locomotion and that habitual grounded running in birds can be understood from that perspective.

The first energy savings strategy is to maintain as columnar a midstance posture as possible (27), reducing the required joint moment to resist gravity. A second strategy for energy savings is to run

with higher DF: Distributing the vertical impulse of the GRF over more time enables lower peak GRFs and lowers rates of force production in the muscles, both reducing metabolic costs (4, 65, 67) and also fatigue (25). However, the second strategy also has mechanisms that increase energy costs and fatigue: The prerequisite crouched postures require higher joint torques and muscle forces (27). The second strategy, thus, represents a trade-off between minimizing peak muscle forces and rate of force development. Humans, despite being tuned for crouched postures (42), can avoid this trade-off because our COM is situated directly above our legs, and thus a near-vertical leg posture is possible (the first strategy).

Birds cannot make use of the first strategy: A vertical leg posture is impossible because of the COM placement in front of the hip (40, 44). In ratites, COM placement is closer to the hip than in volant birds (Fig. 2B) (44), but a human-like posture is still impossible: Our cadaveric manipulations revealed that full knee extension in the emu is limited by as much as 42° (fig. S8), similar to that in ostriches (68). Thus, most birds cannot save energy by adopting (human-like) extended or columnar postures, and they are anatomically and mechanically forced into crouched postures. Because reducing muscle activity by adopting columnar poses is not an option, the second energy savings strategy (running with higher DF) can start to dominate, depending on how the trade-off between peak muscle force and rate of force development balances out. Our simulations show that for birds, grounded running is optimal over a wider range of speeds at increasingly crouched postural tunings (Fig. 6, C and D, left to right).

While systematic evaluations of muscle tunings and optimal joint postures have been presented for certain bird species [e.g., guineafowl (41)], it is currently unknown how these vary across different species of bird. However, crouched poses are a feature of most extant birds, with some outliers and a tendency to adopt less-crouched postures with increasing size (13). Birds appear to be capable of generating forces over wide joint ranges: Similar to (23), we have observed ratites habitually standing up from very deep squatting postures. Given that muscles are strongest at the midpoint of their range, wide active joint ranges imply somewhat crouched optimal poses for most birds. In crouched birds, the trade-off between minimizing peak muscle force (columnar) and rate of force development (crouched) shifts toward the latter: These are the postures near which its muscles can most effectively generate the required moments (41), and this effect apparently dominates. This is why our crouched model variants (and the "wide range" model) adopted grounded running so frequently (Fig. 6 and fig. S6). This also suggests that the narrow grounded running speed range in the ostrich (5), contrasted by the wider speed range in smaller birds (31, 32, 45), can be partially attributed to postural tuning: Bird leg postures become increasingly columnar at increasing body sizes (13, 29).

It is important to point out that habitual postures of animals are determined by more factors than just the posture that maximizes muscle forces (41, 57, 69, 70). This is especially true when joint moments are low (e.g., standing or walking): Passive structures, such as described for the ostrich ankle joint (71) and flamingo knee joint (72), are likely to influence habitual postures. In contrast, at higher speeds, long extensor tendons that stretch under loads lead to not only wider joint operating ranges (9, 19) but also a more flexed midpoint (41) (Fig. 3). Postural control also has a neural component: Guineafowl adopt more crouched postures after undergoing surgery that eliminates proprioceptive feedback from their ankle extensors

(69). Given the large variation in bird COM locations (44, 73) and covarying effects of size and posture (13, 29), it is likely that these factors interact in determining optimal running styles, and these interactions can be challenging to interpret. For instance, studies have shown that when using weights to move the COM of chickens closer to the hip, postures can become both more crouched (74) and more columnar (70), with presumably opposite effects on running styles. Crouched birds also tend to have small body sizes (13, 29), whereas small body size has been suggested to result in higher DFs during running of very young human children (75).

By focusing solely on postural tuning effects in a single bird species (the emu), we were able to eliminate these potential confounders. Overall, our analysis provides an elegant explanation for why it is advantageous for a bird to habitually adopt grounded running: Bird muscles function optimally in relatively crouched postures, and birds are physically incapable of running with (near) vertical limbs. In that situation, they make the best of it by adopting high DFs. Hence, we argue that grounded running in birds is not paradoxical: It is an attractive running style for crouched bipeds. Given the potential interactions between COM placements and postures, it could be illuminating to investigate grounded running in some more columnar species [e.g., the secretary bird, *Sagittarius serpentarius*, for which a SLIP model has been used to characterize aerial running gaits (76)].

How did grounded running in birds evolve?
Birds are direct descendants of (non-avian) theropod dinosaurs, who relied heavily on their massive tails to power locomotion (77–79). Birds lost this massive tail—and resulting cranial shift in COM likely contributed to more crouched postures being required to stand in equilibrium (44). Our analysis implies that this cranial shift in COM was also accompanied by a strong preference for grounded running at intermediate speeds.

Given the similar morphologies, grounded running may have already occurred within the non-avian theropods. Unlike birds, non-avian dinosaurs are often thought to have adopted (relatively) columnar limb poses (78). Although this could suggest that they avoided grounded running, their COM is often reconstructed to lie in front of the hip (44, 80). This situation resembles our columnar model variant, which adopted grounded running (albeit on a much narrower range of speeds than the crouched model variant; Fig. 6). Fossil footprints of dinosaurs demonstrate a smooth distribution in stride lengths, which provides an independent line of evidence for non-avian theropod grounded running (81). Slightly problematic in this regard is that grounded running and smooth gait transitions are not always seen together [e.g., gait transitions in the ostrich are not smooth (21); see also Fig. 6A, elastic crouched].

Grounded running may also be more attractive at large sizes: *Tyrannosaurus rex* was observed to have adopted grounded running in predictive simulations similar to ours, although the gait only occurred at speeds where skeletal stress was higher than physiologically sustainable (77). Empirical data in large quadrupeds also seem to support this possibility: Elephants are known to adopt running without an aerial phase (82, 83).

Future simulation work on extinct taxa would be required to untangle the effects of COM location, leg posture, and body mass reduction on the evolutionary history of birds. Soft tissue information is often lacking in biomechanical analyses of extinct taxa (54, 79, 84), but our simulations are encouraging in that respect: Despite numerous simplifications regarding the contractile and other soft tissue anatomy, our simulations are able to capture salient features of emu gait dynamics (Figs. 4 and 5). Our results suggest that although muscular uncertainties can affect the transition speeds and maximal performance, many spatiotemporal variables (such as stride lengths) are relatively unaffected and remain similar to experimental data.

Complexities in animal gait selection
It is frequently recognized that animals select steady-state gaits with low MCOT (2, 5, 6). However, the mechanism through which animals sense MCOT remains unclear, and peak muscle activations [which we refer to as fatigue following (24)] have been put forward as a potential proxy for sensing energy costs (11). In simulations with springless telescopic leg actuators, true work-minimal gaits are very impulsive (with low DF and very high peak GRF) (25, 46, 47). We found similar results in our MCOT-only optimizations when using rigid tendons and rejected these for not being representative of real animal locomotion. When using telescopic actuators, a penalty on leg force rates improves realism, which phenomenologically models finite contraction speeds and viscosity of biological structures (25, 46, 47). Such a force-rate cost resembles the "smooth contraction" cost term used here and in previous studies [see the "Cost function" section and (48)] and has similar results to a fatigue or activation cost when simulating periodic locomotion (25): All serve to reduce the (costly) rate of muscle force development (4) and, as a result, increase DF and reduce peak GRF. While there is still debate concerning whether MCOT, fatigue, or a combination of the two is most appropriate of predictive gait simulations (11, 24, 25), grounded running was optimal for our crouched-tuned model using all three possible cost functions.

Currently, relatively little information exists regarding how animals choose their gaits when changing speeds. It has been suggested that peak musculoskeletal forces can trigger gait transitions (16), which, in our simulations, can be interpreted as a cost function that incorporates fatigue. Our approach has modeled changes in the desired speed as an optimization, using the current speed as a starting point. This results in a gait hysteresis; in our simulations, the walk-to-run transition occurs at a higher speed than the run-to-walk transition (Fig. 6), which appears to be phenomenologically valid on the basis of observations in the ostrich (21). However, we do not claim to have modeled the underlying mechanism. The gait hysteresis we found is likely an effect of using gradient-based optimizations, which may lead to minimal changes in gait dynamics when reinitializing subsequent optimizations. Put more simply, sequentially increasing or decreasing the target speed, while using each previous (slower or faster) trial as a new initial guess, likely biases the gaits to be more similar to the previous trial. This is particularly important at speeds where many different gaits are possible without a large change in MCOT or fatigue.

Our simulations provide an energetic mechanism that explains a preference for grounded running that is dependent on postural tuning. However, we have only modeled steady-state, level locomotion, which does not encompass the full locomotor repertoire of animals (9, 14, 21). Emus habitually switch between walking and running midstride over a range of submaximal speeds (6), and ostriches show considerable overlap between their walking and running speeds (21). These and other observations suggest that animal gait selection may be situation dependent, and many factors beyond MCOT are likely to play a role (11, 12, 14, 16, 35, 69). Grounded

running has many other benefits to the organism: A large range in effective leg length (or high "leg compliance") increases stability against perturbations (*35*) and may contribute to the capacity of birds to maintain consistent leg forces when running on uneven terrain (*14*), which is thought to be an injury prevention strategy. From this perspective, simulations of our "wide range" model shows that crouched poses may be an effect of requiring wide active joint ranges in daily life, because of the numerous benefits it confers to the avian body plan. These and other benefits could make grounded running attractive for bioinspired robotics (*64*, *85*).

Limitations

In our view, the purpose of a model is to answer questions related to complex phenomena in nature. For a model to be useful, it must isolate the aspects of reality that are key to addressing the questions at hand while eliminating unnecessary complexity. We did not set out to perfectly model all aspects of emu locomotion. Our goal was to elicit different running styles by systematically changing the anatomy of our model. Modeling the true anatomical complexity of emus would, thus, have been counterproductive to this goal. This section explains why certain simplifications were made, discusses their implications, and points out other limitations of this study.

We have modeled walking and running as pure (para)sagittal plane movements using hinge joints, a common modeling choice (*24*, *25*, *40*, *54*). This greatly improved the controllability of our model, enabling a much larger scope for our analysis (more than 650 simulation trials). Such a large scope was required to decouple the many mechanical factors related to gait transitions. It has been shown that ratite joints display clear out-of-plane movements, particularly at the hip joint which is externally rotated throughout the stride (*86*). However, the resultant moments about the global x and y-axes (see Fig. 2) have been proposed to (partially) be counteracted by passive structures (*38*), and the mediolateral component of the GRF does not vary systematically with speed in birds (*29*). Hence, modeling these out-of-plane movements appears not to be necessary to predict overall gait dynamics, which is bolstered by the close match between our simulations and measured gait metrics in emus (Figs. 4 and 5).

Our model also does not permit any movement in the metatarsophalangeal (MTP) joints. Our study design included a comparison between the effects of elastic and rigid tendons, while keeping other contractile parameters constant. This would be incompatible with a mobile MTP joint: In ratites, flexion and extension of the MTP joints are thought to be facilitated by elastic storage in the digital flexor tendons (*38*), similar to guineafowl (*9*). Although the MTP joints show the largest joint excursions during the stride, this occurs predominantly during the swing phase (*30*, *86*). The GRF progressions of our models (Fig. 4) demonstrate that omitting the MTP joint does not prevent realistic foot-ground interactions, and thus overall stance-phase dynamics, which seem most relevant to grounded running. Although we did not simulate MTP joint flexion and extension, this joint is incorporated in our model using a locked joint (WeldJoint in OpenSim) that could be unlocked in future studies.

Our study design hinged on systematically changing the postures in which the muscles in our model could generate peak forces, enabling us to investigate how this affected optimal running styles. We therefore did not model the functional specializations in muscular architecture and other passive structures recognized in ratites because those could potentially bias optimal postures and gait selection in our simulations. Thus, several adaptive features linked to low MCOT in ratites and birds are not included in our model: Ratites have ankle ligaments that generate moments leading to two stable joint poses (*71*) and digital flexors that store large amounts of energy during the stride (*9*, *19*, *38*, *64*). Emu hindlimb muscles are also metabolically and structurally highly specialized for sustained high-speed running (at low energy cost) (*20*, *37*, *63*), which is not represented in our model (Fig. 2). Lumped parameter Hill-type muscles may overestimate fiber length changes (*87*), which, in our methodology, would lead to weaker muscles when keeping muscle mass constant (Eq. 1).

It would be reasonable to assume that our model would underestimate the locomotor performance of emus by omitting these features. It may then seem unexpected that most of our model variants have lower MCOT than reported for emus (*6*). This is likely due to a combination of effects. Our model does not require any muscle activations for lateral stabilization (see above). Total MCOT also includes the metabolic costs of nonlocomotor functions (e.g., faster heartbeats, the digestive system, etc.) that comprise the basal metabolic rate (BMR). When estimating MCOT (*88*), we used a "true" BMR of 0.92 W kg^{-1} measured in emus in a darkened chamber at night (*89*). However, the metabolic rate of emus when standing (during daytime) has been reported as ~2 W kg^{-1} (*6*). Using this higher estimate of BMR would result in higher MCOT at lower speeds, where BMR is a larger proportion of total MCOT. We also tuned our model variants for narrow joint ranges to deliberately bias it toward specific postures—using wide joint ranges would prevent us from performing the main analysis (see the "Muscle contractile parameters" section). At a fixed muscle mass, these narrow joint ranges result in relatively short fibers (low L_O), which, per Eq. 1, leads to strong muscles (high F_{max}). This effect is strengthened because we mapped individual muscle masses onto functional groups in the sagittal plane. Hence, the values of MCOT in Fig. 6C are underestimates. Our "wide range" model from the sensitivity analysis shows that a wider tuning range results in higher MCOTs (fig. S6). To accurately model all aspects of ratite locomotor performance simultaneously (wide active joint ranges, high top speed, and low MCOT), it may be necessary to model all muscles individually or even split up each muscle further [e.g., (*41*, *55*)], substantially complicating the control procedure and increasing computational time. Muscle power output in mice decreases under repetitive contractions (*90*), and similar experiments have not been performed on ratite muscles. Hence, we currently lack sufficient anatomical and physiological information to simultaneously capture all aspects of ratite muscle functioning using computational models.

Last, as is often the case with simulation studies, it is impossible to guarantee global optimality of the presented gaits, demonstrated by the differences between our walk-to-run and run-to-walk optimizations discussed previously. We have taken numerous steps to investigate the robustness of our claims, including systematically searching for alternative walking solutions, approaching the gait transition speeds from two directions, and investigating the effect of different cost functions. A recurring pattern in all of these investigations was that models tuned for crouched postures adopted higher DFs.

Despite these limitations, our emu model variants enabled us to isolate the effect of different aspects of their musculoskeletal design on overall gait dynamics. By simulating grounded running with

rigid tendons, we demonstrated that grounded running does not require elastic storage, although grounded running is facilitated by elastic tendons through their effects on leg postures. Mechanically, grounded running gaits require larger variations in effective leg length during the stance phase than aerial running—this is easiest to achieve with a crouched posture. More generally, we found that models that were strongest in crouched postures adopted crouched running gaits with higher DFs than columnar models. Thus, while columnar postures enable lower joint torques (and thus lower muscle forces), columnar running is only advantageous when the muscles function optimally in these postures. Humans are an exception in this regard because we can stand in equilibrium when we fully extend all of our joints. In birds, a fully extended posture is impossible because of the forward placement of the COM. Integrating these findings, we reject the existence of a grounded running paradox in birds. We conclude that birds adopt grounded running because it is the most energetically advantageous gait that is available to them at intermediate speeds.

MATERIALS AND METHODS
Overview
We constructed a generalizable (i.e., not subject-specific) 3D musculoskeletal model of the emu for use in predictive physics simulations. The model incorporates all the unique mono- and biarticular (sagittal plane) muscle functions of emus (20, 37), while combining muscles with identical functions into functional groups. We systematically varied the muscle contractile parameters so peak muscle forces in the model occurred in three different postures (combinations of joint angles): columnar (albeit less extended than humans), intermediate, and crouched (Fig. 3). For each of these three postural variants, we considered the effects of both rigid and elastic tendons, resulting in six model variants in our main analysis.

Using optimal control theory, we optimized gaits for the model variants, across their entire speed ranges. Our simulations were acquired without using movement data from emus as an input. Systematic differences between model gaits thus reflected differences in musculoskeletal design—postural tuning and/or tendon elasticity—of the models. To validate simulator outputs, we visually compared them to published gait data of real emus (GRFs, stride lengths, and DF).

Because optimizations can be sensitive to initial conditions, we simulated gait transitions in two directions. For the "walk-to-run" modality, we started the sequential optimizations at walking speed, and we increased the target speed for subsequent trials by 0.5 m s^{-1} until we found the model variant's top speed (see movie S3). For the "run-to-walk" modality, we started the optimizations at top speed, and we decreased the target speed for each trial in steps of 0.5 m s^{-1}. Each trial used the previous trial from the sequence as the initial guess for the optimization at the new target speed.

In the simulated gait transitions acquired in this way, we compared how postural tuning and tendon elasticity affected the occurrence of grounded running and corresponding metrics of MCOT and muscle fatigue. We also performed extensive sensitivity analyses to investigate the robustness of our claims to implementation choices. This included the inclusion of alternative cost functions (in the optimizer) and several attempts to acquire aerial gaits at speeds where grounded gaits were optimal, and vice versa. In total, we analyzed the results of over 650 optimizations. We uploaded code

examples, all model variants, and simulator outputs to our SimTK project page, an open biomechanics repository (see Data and materials availability).

Inertial parameters
We acquired a computed tomography (CT)–based 3D model of an emu skeleton from (44). We imported the 3D models into Blender 3.0 (blendernation.org, open-source 3D modeling software). To account for the posture it was scanned in, the skeleton was reposed into a neutral position, and the torso was slightly symmetrized (Fig. 2A, top). We then applied a validated convex hulling procedure (in Blender) to estimate the inertial parameters directly from the skeleton (44). The basic procedure is as follows:

1) Generate minimal (3D) convex hulls around distinct body segments as defined in (44);

2) Scale the hulls using segment-specific scale factors validated in birds (44), so that it represents the skin outline; the skeleton was not perfectly symmetric—we generated symmetric hulls by mirroring the right-side to the left-side, while accounting for the change in volume due to this extra step;

3) Multiply the volumes and volumetric inertia tensors by segment density to obtain the mass properties.

We used the average (isometric) bird convex hull expansions from (44). Expanding the torso as a single segment redistributes an inappropriate amount of volume around the ribcage. After computing the total torso volume as predicted by their equations, we split the unexpanded torso hull into a pelvic portion and a ribcage portion. We only expanded the ribcage portion enough to ensure that the symmetrized hull enveloped the skeleton. The rest of the torso volume was accounted for by expanding the pelvic portion. Splitting up the torso segment in this way results in a torso skin outline that more closely resembles the CT-based skin outlines (44), where the pelvis is much wider than the ribcage. To more closely match the proximal concentration of mass in the thigh and shank segments of emus, the corresponding hulls were only expanded on the proximal ends until the target volume was achieved. The final hulls are shown in Fig. 2A (bottom). All hulls were assigned a density of 1000 kg m^{-3}, except for the head, neck, and torso hulls, which were assigned a density of 888 kg m^{-3} (80), and the calculated body segment parameters are presented in Table 1. Estimated body mass was 37.8 kg, which was within 1% of the mass measured using scales (38.1 kg) for the same individual (44).

Muscle masses
We compiled a dataset of body mass–normalized muscle masses of the average adult emu hindlimb, based on published data. Lamas *et al.* (37) reported two large datasets, ranging from hatchlings to adults, which we combined with an adult measurement from Goetz *et al.* (55). We adopt the standardized nomenclature of the Handbook of Avian Anatomy (91), but some of the data followed nomenclature of Patak and Baldwin (20). These nomenclatural inconsistencies are also present in ostrich myology, briefly discussed in (57). We converted all the data to a single naming convention and excluded uncontroversially juvenile specimens (based on muscle mass; see Supplementary Text and fig. S9). This muscle mass dataset is based on 28 specimens (body mass range, 15.6 to 51.7 kg), with sample sizes varying per muscle (table S1). The median sample size was $n = 19$ (for nine muscles), the lowest was $n = 9$ [M. ischiofemoralis, which is a diminutive muscle that is challenging to dissect; see (37)], and the highest was $n = 28$ (for six muscles). Hindlimb

Table 1. Inertial parameters of the emu model body segments. COMs are reported with respect to the midpoint of the two hip joint centers, in the reference pose depicted in Fig. 2B. Mass moment of inertia (*I*) tensor elements are reported about the COM of each segment. The model is symmetric about the *xy*-plane, and only the right limb is reported. For a full model specification, the reader is referred to the .osim and raw .txt files provided on our project page (see Data and materials availability).

Rigid body	Mass (kg)	COM (m)	$I_{xx}, I_{yy}, I_{zz}, I_{xy}, I_{xz}, I_{yz}$ (kg·m^2)
Head, neck, forelimbs, and torso	23.929	(0.162, −0.023, 0.000)	(0.466, 1.24, 1.62, −0.46, 6.77×10^{-10}, -4.52×10^{-10})
Thigh (right)	3.512	(0.017, −0.069, 0.094)	(0.0171, 0.0101, 0.0205, 0.000479, −0.000651, −0.00036)
Shank/tibiotarsus (right)	2.711	(0.024, −0.352, 0.082)	(0.033, 0.00357, 0.0334, −0.00123, 4.99×10^{-5}, -2.99×10^{-5})
Foot—midfoot/tarsometatarsus (right)	0.551	(0.018, −0.810, 0.084)	(0.00688, 0.000132, 0.00684, 3.72×10^{-5}, 2.18×10^{-6}, 0.000108)
Foot—toes/phalanges (right)	0.161	(0.080, −1.016, 0.085)	(0.000131, 0.000329, 0.000246, 5.7×10^{-5}, -2.27×10^{-6}, 6.57×10^{-6})
Total (bilateral)	37.799		

muscle mass of emus (raised in captivity, excluding juveniles) in this dataset is, on average, 14.9% of total body mass (per limb), nearly identical to the 15% reported in Lamas *et al.* (*37*) based on a subset of their own data. The highest percentage (16% body mass per limb) was found in a specimen from their UK dataset at a body mass of 42 kg (*37*). Patak and Baldwin (*63*) report ankle extensor muscle masses for wild emus, which, on average, are 7% heavier than the captive emu dataset presented here.

The 34 muscles listed in table S1 have considerable functional specializations due to their varying architecture (*20*, *37*, *63*). Our study design relies on biasing the model toward specific poses, representing the real functional complexity of the muscular system that is counterproductive to this goal (extensively discussed in the "Limitations" section). Furthermore, our model only incorporates sagittal plane movements because mediolateral forces do not vary systematically with speed in birds (*29*). Therefore, we mapped the 34 muscles of the emu hindlimb onto five monoarticular functional groups and four biarticular functional groups, which we consider the major muscle functions in the sagittal plane. These functional groups, body mass–normalized muscle masses, and the anatomical muscles they are based on are presented in Table 2. Figure 2B shows the corresponding muscle lines of action, which were constructed using comparisons with existing ratite models (*55*, *57*) and a 3D surface scan of a *Rhea* plastinate with the muscles preserved in situ.

When a unique mapping was not appropriate, muscle masses were distributed evenly over multiple functional groups (Table 2 and Supplementary Text). Table 2 includes a sixth monoarticular muscle [knee flexion by M. femorotibialis medialis (*22*, *37*, *57*)]. Its topographical arrangement suggests that it is predominantly a knee adductor (or stabilizer), but some authors have also classified it as a (weak) knee flexor (*37*, *57*). Given this uncertainty in the literature, we added its muscle mass to the "hip extensor knee flexor" functional group for all the results of the main analysis. We investigated its effect as a monoarticular flexor in the sensitivity analysis.

Muscle contractile parameters
Our goal was to assess how habitual limb postures affect locomotor dynamics. We achieved this by generating model variants with contractile parameters of the nine muscle-tendon units tuned for

different postures. In animals, muscle fibers operate over relatively narrow length ranges in vivo and cannot actively generate large forces outside of these ranges (*10*, *43*). Optimal lengths of the muscle fibers, combined with dynamic interplay with the tendons, are highly determinant of habitual limb poses and joint ranges (*10*, *41*, *43*). Similar to previous animal simulation studies (*54*, *56*, *58*, *77*), we tuned our model using specific joint ranges (and thus postures) using the length changes of the muscle in different postures to determine fiber and tendon lengths (explained in detail below).

We chose three limb postures (see Fig. 3 and movie S2): columnar (relatively extended joints), intermediate, and crouched (flexed joints). These postures were not intended to match emu joint angles, but instead represented a suitably wide postural gradient to allow us to investigate the effect of posture on gait selection. We did not allow joint hyperextension. Because muscles generate the highest forces at the approximate midpoint of their range, to be able to generate a columnar variant at all, it was necessary to choose relatively narrow joint tuning ranges. However, if joint ranges are too narrow, fiber lengths take on unrealistically low values (see below). After pilot testing, we found joint tuning ranges of 45° (hip), 65° (knee), and 70° (ankle) to represent a reasonable compromise (slightly more than half the unresisted passive joint ranges).

Compared to joint excursions in walking and running ratites (*30*, *55*, *71*, *86*), our joint tuning ranges are twofold wider at the hip [but similar to (*30*)] and slightly narrower (~15°) at the ankle. This was a necessary departure from bird behavior to enable a systematic comparison of the effect of habitual posture on locomotion. To investigate the effect of this, we considered a model tuned for much wider active joint ranges as a sensitivity analysis (see the "wide range" model variant in the "Sensitivity analyses" section).

We modeled the muscles using three-element Hill-type muscles, incorporating first-order activation dynamics (*92*, *93*). A muscle fiber is represented by a contractile element (CE) and a nonlinear parallel elastic element (PEE) and generates the highest isometric force at its optimal fiber length (L_O; in meters). For the elastic tendon variants, tendons are represented by a nonlinear series elastic (SEE) element, with a corresponding tendon resting length (L_T; in meters). The fiber and tendon are placed in series to represent a whole muscle.

Table 2. Functional groupings in the model. Functional muscle group masses in the model are based on average emu hindlimb muscle masses from Lamas *et al.* (*37*) and Goetz *et al.* (*55*) and are reported normalized to body mass. See table S1 for individual muscle masses. Muscle masses were distributed over multiple functions when a singular mapping was not appropriate.

Muscle function	Body mass–normalized mass	Muscle mass based on	Line of action based on
Hip extensor	0.0128	Caudofemoralis pars pelvica, Pubo-ischio-femoralis partes laterales et mediales, Flexor cruris lateralis pars accessoria, Iliotrochantericus cranialis (50%), Iliotrochantericus medius (50%), Iliotrochantericus caudalis (50%), Ischiofemoralis (50%)	Caudofemoralis pars pelvica
Hip flexor	0.0103	Iliofemoralis externus, Iliofemoralis internus, Obturatorius medialis partes ilioischiadicae et ischiopubicae, Iliotrochantericus cranialis (50%), Iliotrochantericus medius (50%), Iliotrochantericus caudalis (50%), Ischiofemoralis (50%)	Iliotrochantericus caudalis
Knee extensor	0.0114	Femorotibialis lateralis, Femorotibialis intermedius	Femorotibialis lateralis
Knee flexor (sensitivity analysis only)†	0.00269	Femorotibialis medialis†	Femorotibialis medialis†
Ankle extensor	0.0302	Gastrocnemius pars medialis, Flexor digitorum longus, Fibularis longus	Gastrocnemius pars medialis
Ankle flexor	0.00750	Tibialis cranialis capita femoralia et tibialia, extensor digitorum longus	Tibialis cranialis caput tibiale
Hip flexor knee extensor	0.0162	Iliotibialis cranialis, Iliotibialis pars preacetabula-ris*, Ambiens (33%)	Iliotibialis cranialis
Hip extensor knee extensor	0.0133	Iliotibialis pars postacetabularis*, Ambiens (33%)	Iliotibialis pars postacetabularis
Hip extensor knee flexor	0.0229	Iliofibularis, Flexor cruris lateralis pars pelvica, Flexor cruris medialis, Ambiens (33%)	Iliofibularis
Knee flexor ankle extensor	0.0214	Gastrocnemius pars lateralis, Gastrocnemius pars intermedia, Flexor hallucis longus, Flexores perforati digiti II, III, et IV, Flexores perforantes et perforati digiti II et III	Gastrocnemius pars lateralis
Total	0.149		

*We used the measurements reported by Goetz *et al.* (*55*) to split up masses of Iliotibialis partes pre- et postacetabulares (29% and 71% of the total, respectively).   †Femorotibialis medialis mass was added to the "Hip extensor knee flexor" in all model iterations used in our main analysis and was only modeled separately in sensitivity analysis 3, where we simulated a knee flexor model variant.

We set L_O of each muscle fiber so that it extends between 0.5 and 1.5 when the joints are moved over the tuning ranges. For the columnar model variant, we set the midpoint of these ranges at 22.5° (hip), −47.5° (knee), and 40° (ankle). L_T was determined by subtracting L_O from the total muscle length at these midpoints. We biased the model toward intermediate and crouched postures by shifting the midpoints by 10° and 20°, respectively, and recalculating L_O and L_T. The tuning ranges were only used to construct the models, and during gait optimizations, the models were free to adopt a much wider range of joint angles. However, these tuning ranges achieved systematic differences in posture between conditions, which was our goal.

Maximum isometric force (F_{max}; in newton) was dependent on the muscle's mass (m_{muscle}; in kilograms) and L_O using Eq. 1

$$F_{max} = \frac{m_{muscle}\sigma}{\rho L_O} \quad (1)$$

Here, σ is the specific tension of muscle tissue (0.3 MPa used here) (*54*, *56*, *77*), and ρ is the density of muscle tissue (1060 kg m^{-3}). We do not explicitly model the pennation angle because the functional

muscle groups in our model represent the combined effect of several muscles.

Given that we prescribed m_{muscle} for each muscle, Eq. 1 shows that F_{max} is inversely proportional to L_O: A muscle with short fibers has a larger maximal force, and vice versa. Our deliberate choice for relatively narrow joint ranges therefore likely increases F_{max}, causing a systematic underestimation of MCOT. We investigate this effect in the sensitivity analysis ("wide range" model variant).

For the elastic tendon model variants, tendon strain at F_{max} was set to 4%. Similar to (*41*, *58*), L_T was kept constant between the rigid and elastic tendon variants to directly compare the effect of tendon elasticity.

Model construction

We treat the head, neck, forelimbs, and torso as a single rigid body (Table 1). The model has bilaterally symmetric rigid bodies representing the thigh, shank, and foot bodies, resulting in three-segment legs. The foot body is made up of the midfoot (tarsometatarsus) and the toes (phalanges), which cannot move independently from each other—they are fixed in a rigid L-shape (Table 1 and Fig. 2). Joint

locations (Fig. 2B, purple circles) were determined by manually fitting geometric primitives to the articular surfaces in Blender.

All the 3D data (inertial properties, joint locations, muscle paths, and contact sphere locations) were computed in Blender and then converted for simulations in OpenSim 4.4, open-source software for biomechanical analysis (94). We constructed the model using the OpenSim API in MATLAB R2019b (MathWorks, Natick). We constrained the "head, neck, forelimbs, and torso" body to the sagittal plane (three degrees of freedom), and all other joints were hinge joints, leading to nine degrees of freedom in total. We did not include any passive joint stiffness or damping in the model.

The model has nine controllable muscles per hindlimb. We used the muscle model described by De Groote et al. (52) [implemented in OpenSim as "DeGrooteFregly2016Muscle" (60)]. Parameters that were kept constant for each muscle throughout our experiment are maximal contraction velocity [14 L_O s^{-1}, based on turkeys (95)], activation time constant (15 ms), deactivation time constant (60 ms), and PEE strain at F_{max} (60%).

The model has 10 ground contact spheres per foot (0.015 m in radius). Contact forces were modeled using a smoothed Herz-Hunt-Crossley model, as described in (49) [implemented in OpenSim as SmoothSphereHalfSpaceForce (60)]. Plane strain modulus was set to 2.5 MPa, dissipation to 0.2 s m^{-1}. Static and dynamic friction coefficients were set to 0.4, and viscous friction was set to 0.1 to prevent slippage at higher speeds. The "herz_smoothing" parameter was set to 600. Model specification files (in .osim format) of all our model variants can be found in on our SimTK Project page (see Data and materials availability), which can be interactively posed and examined in OpenSim 4.4.

Optimizations

In our model, the only controllable inputs are the open loop neural inputs (excitations), one for each muscle, with no model state feedback. Excitation results in muscle activation (via first-order activation dynamics). Each muscle's force production depends on its instantaneous fiber length and velocity, and its activation. The time-dependent neural inputs of all the muscles together must result in periodic locomotion. Finding appropriate neural signals for periodic gait was traditionally extremely computationally costly (54, 56). These neural signals are commonly found using optimal control: The gait of the model can be optimized by assuming that animals select their gaits by minimizing one or several objectives (11, 24, 25, 48, 54, 60).

Optimizations that include MCOT as the only (main) objective often do not produce realistic motions (24, 51) because they do not equally distribute loads over all the available muscles. By minimizing the neural input to the muscles raised to a power, muscle activity is distributed more equally across the muscles (irrespective of size), often resulting in more realistic gaits (24). Ackermann and van den Bogert (24) referred to such a cost function term as "fatigue" and "fatigue-like" because it is thought to represent fatigue sensing in the muscles. Similar to previous research (11), we adopt this narrow definition of the term fatigue in this manuscript (i.e., neural excitations cubed; see the "Cost function" section). However, broader, context-dependent definitions of the term fatigue also exist (96). While there is evidence that in certain situations, fatigue dominates over MCOT in gait selection (11), there is currently no consensus on their individual contributions in animals [see also the extensive discussions regarding cost functions in (25)]. Therefore, we used three

different objectives for our optimizations: (i) fatigue and MCOT, (ii) fatigue only, and (iii) MCOT-only. Our main analysis focuses on the combined fatigue and MCOT optimizations.

Recently, direct collocation has gained popularity as a control approach with greatly reduced optimization times (24, 48, 52, 60). Direct collocation differs from more traditional simulation workflows because trials are not acquired through forward integration over time. Instead, all the time points of the simulation are optimized simultaneously, and system dynamics are enforced as equality constraints that can initially be ignored during the optimization. We will refer to our converged optimizations (i.e., gait trials) as simulations (24, 43, 48). We implemented direct collocation using the optimization suite Moco (in OpenSim) to acquire biologically realistic gaits for our model (60). We set convergence and constraint tolerances in Moco to 10^{-3} and 10^{-4}, respectively.

Cost function

We implemented a multiterm objective function, similar to (48)

$$C = \int_0^T \left(\underbrace{w_1 \frac{\sum_{m=1}^{N_M} |U_m|^3}{N_M \, d}}_{\text{Fatigue}} + \underbrace{w_2 \frac{\sum_{m=1}^{N_M} \dot{E}_m}{M_{Tot} \, d}}_{\text{MCOT}} + \underbrace{w_3 \frac{\sum_{m=1}^{N_M} \dot{F}_{T,m}^2}{N_M \, v_{p,x}}}_{\text{Smooth contractions}} + \underbrace{w_4 \frac{\sum_{i=1}^{N_I} \ddot{q}_i^2}{N_I \, v_{p,x}}}_{\text{Smooth motions}} \right) dt \quad (2)$$

Here, w_1 to w_4 are the weights for scaling the four terms in the cost function; T is the final time point (in seconds) of the simulation; N_M is the number of muscles; N_I is the number of coordinates (degrees of freedom); U_m is the control input (excitation) of muscle m, bounded between 0.0001 and 1; d is the distance traversed (in meters) in x direction by the pelvis between $t = 0$ and $t = T$; $v_{p,x}$ is the average velocity (in meters per second) in x-direction of the pelvis; M_{Tot} is the total body mass (in kilograms); $\dot{E}_m$ is the total metabolic rate (in watts) of muscle m; $\dot{F}_{T,m}$ is the time derivative of the normalized tendon force of muscle m; and $\ddot{q}_i$ is the second time derivative of coordinate i.

Weight w_1 was kept constant between all model variants. Weight w_2 was selected so the contributions of fatigue and MCOT were approximately equal at 1.25 m s^{-1}. The smoothness criteria w_3 and w_4 are typically used to improve numerical conditioning (48). They also serve to limit tendon oscillations (when using elastic tendons) and jittery gaits. We scaled w_3 and w_4 so that their respective contributions to C were small (<10% of the muscle fatigue at 1.25 m s^{-1}). All weights were kept constant for all the speeds considered. w_3 was zero in the rigid tendon simulations. The velocity terms multiplied by w_3 and w_4 ensure that their relative contributions are somewhat constant irrespective of the speed, but a systematic treatment of cost-function scaling goes beyond the scope of the current study. To account for this, we also ran the optimizations without MCOT and without fatigue included (w_2 and w_1 set to zero, respectively), and in sensitivity analysis 4, we rescaled w_1 and w_2 at 3.25 m s^{-1} (grounded running speed).

MCOT was estimated using the phenomenological model proposed by Bhargava et al. (88), assuming a 50% distribution in slow and fast muscle fibers. We set the BMR to 0.92 W kg^{-1}, the mean of all emu measurements reported in (89), assuming 20.1 J of energy released per milliliter of oxygen consumption (3).

Each half stride was discretized into 101 time points. This has the desirable effect of automatically decreasing the simulation time

steps at faster target speeds because the stride periods become progressively shorter.

Constraints

We enforced target average speed in x-direction and also enforced periodicity and bilateral cross-symmetry of coordinates and muscle excitations. This results in half strides where the initial states and controls of the right side match the final states and controls of the left side, and vice versa. We transformed these half strides into full strides by placing a bilaterally mirrored trajectory in sequence with the original. For an arbitrary state S that has a left and right variant, the constraints to acquire the half strides can be written as

$$S_{R,t=0} = S_{L,t=T} \qquad (3)$$

$$S_{L,t=0} = S_{R,t=T} \qquad (4)$$

We further placed lower and upper bounds (b_L and b_U, respectively) on all state variables defining position (q) and velocity ($\dot{q}$)

$$b_L \leq \begin{pmatrix} q \\ \dot{q} \end{pmatrix} \leq b_U \qquad (5)$$

Apart from the constraint on pelvis angle, these bounds were wide enough to remain inactive in all of the converged solutions but served to reduce the size of the search space. These bounds do not represent mechanical constraints on the model—no constraint forces would occur if the bounds are reached. Instead, these bounds should be interpreted as limits on acceptable joint poses and speeds, which must be satisfied by the controller.

Gait generation

We first generated optimal walking gaits at a target speed of 1.25 m s^{-1} [close to preferred walking speed of emus (6)], using two initial guesses for each model iteration: (i) a dynamically consistent, static balance simulation and (ii) a dynamically inconsistent, "quasi-random" guess (48), where the model floated forward at the target speed with swinging limbs. Both initial guesses sometimes resulted in nonoptimal gaits (e.g., hopping, skipping, and marching). Some examples of these are provided in movie S4. These local optima were avoided somewhat by initially placing tight bounds on the coordinate speeds and T—these bounds were lifted once a good walking solution was found. We also implemented a procedure similar to "gait morphing" (54), reinitializing the optimizer with a (portion of a) converged solution as a new initial guess.

For each of the two walking solutions found per model, we further investigated whether enforcing stride lengths between 0.75 and 1.75 m (in steps of 0.25 m) would lead to better solutions (because we have a multiobjective cost function). We also cross-checked solutions for the different model variants if we suspected a local optimum. Overall, we generated at least 12 viable solutions per main model variant, before selecting the solution with the lowest cost.

We then sequentially increased the target speed in steps of 0.5 m s^{-1}, each time using the previous solution as a "hot start," until we reached a speed at which the optimizer would no longer converge. We refer to this sequence of optimizations as the walk-to-run modality (see movie S3). In these optimizations, the average velocity of the initial guess was always 0.5 m s^{-1} lower than the target velocity,

which could potentially induce a bias in the gait transition speeds. To eliminate this bias, we repeated the procedure in reverse: Using the fastest converged speed (always an aerial running gait) as an initial guess, we sequentially reduced the target speed until 0.75 m s^{-1}. We refer to this sequence as the run-to-walk modality.

Sensitivity analyses

We performed extensive sensitivity analyses in the form of extra model variants and alternative optimization approaches, which we list here (in the same order as the "Sensitivity analysis results" section).

1) Our rigid tendon models still had the potential for some elastic storage in the PEE and the smooth ground contacts. To eliminate the possibility that any elastic storage was required for grounded running, we constructed a "no elastic storage" model variant. This was a rigid crouched model variant without a PEE, and much stiffer (nonsmooth) ground contacts [HuntCrossleyForce, as implemented in OpenSim (97)]. Plane strain modulus was set to 12.5 MPa (five times higher than the base model variants). All other parameters were kept the same.

2) Our main analysis depended on deliberately tuning the model variants for narrower joint ranges than in real life (see the "Muscle contractile parameters" section). To explore beyond this experimental paradigm, we constructed a "wide range" model variant. This model was tuned with much wider joint ranges, approximating the unresisted passive joint range determined through cadaveric manipulation of several ratites (*Dromaius*, *Casuarius* sp., and *Rhea* sp.; see Supplementary Text for details). This model was tuned assuming 85° hip, 115° knee, and 130° ankle ranges (with midpoints at 42.5°, −82.5°, and 70°, respectively). The hip joint range was challenging to measure accurately, and we deliberately erred on the side of overestimation (i.e., widest plausible hip range) when tuning this model, to contrast the model variants in the main analysis that used narrow joint tuning ranges (see the "Muscle contractile parameters" and "Sensitivity analyses" sections and Supplementary Text).

3) The function of M. femorotibialis medialis is currently poorly understood, so our main model variants do not include its potential effect as a monoarticular knee flexor. To investigate its effect during gait, we constructed knee flexor model variants: intermediate and crouched model variants (with rigid tendons) with a knee flexor muscle.

4) We initially scaled the relative weights of fatigue and MCOT in the cost function (w_1 and w_2 in Eq. 3, respectively) at a speed of 1.25 m s^{-1}. However, the cost of fatigue increased more substantially at higher speeds than MCOT. We investigated how reweighting the cost function at 3.25 m s^{-1} (grounded running speed for the elastic columnar and crouched models) would affect the gait optima.

Unless stated otherwise, we used a walking solution of one of the main model variants that most resembled it to generate a new walking solution, before traversing the walk-to-run transition as described above.

Computation of gait metrics

We compared DFs, strides lengths, and GRFs from our simulations to empirical emu data from (17, 28–30, 55, 98) in Figs. 4 and 5 and figs. S1 and S2. In the "Gait transitions and grounded running" section, we also compared our simulations to published measurements of MCOT and gait transition speeds in emus (6). To aid these

comparisons, we computed nondimensional gait parameters as follows: We defined h (in meters) as the average hip height during walking. We computed h as the mean value at a forward velocity of 1.25 m s^{-1} in our simulations, but some of the studies we compared did not report the velocity at which they determined h, or computed it for standing trials. Stride length L (in meters) was defined as the distance between successive footfalls of the same foot. We computed relative stride length $\widehat{L}$ by normalizing stride length to h. Relative velocity $\widehat{v}$ was obtained by dividing forward velocity v (in meters per second) by $(g\,h)^{0.5}$, where g is the gravitational acceleration constant (in meters per second squared). The quantity $(g\,h)^{0.5}$ is also the upper limit on walking for an inverted pendulum. $\widehat{v} = 1$ thus represents a theoretical upper limit on walking gaits, although grounded running at $\widehat{v} > 1$ is possible in the SLIP model (*34*) and is regularly adopted by birds (*29*, *31*, *32*). The Froude number Fr for pendular walking is equivalent to $\widehat{v}^2$ (*1*). Because we only focus on steady-state, forward locomotion, we will use the terms velocity and speed interchangeably.

GRF was reported as a fraction of body weight. DF (fraction of the stride that one or both feet are in contact with the ground) was determined on the basis of the presence of intersections between contact spheres and the ground.

To compare stance phase dynamics between model variants, we defined effective leg length L_{eff}: the average distance (in meters) between the point of net vertical force application (calculated while neglecting fore-aft forces) and the hip joint during the stance phase. To focus our comparison on the walk-to-run transition, we computed the average over a speed range of 1.25 to 3.25 m s^{-1}. We report maximum and minimum values, normalized to the average ($L_{\text{eff}+}$ and $L_{\text{eff}-}$, respectively).

DF and $\widehat{L}$ measured in emus from (*28*, *30*) were digitized using WebPlotDigitizer 4.0 (https://apps.automeris.io/wpd4/) to supplement the emu data from (*29*) in Fig. 5. Force-plate and kinematic data of emus were shared with us by J. Hutchinson [from (*29*, *98*)], J. Goetz [from (*55*)], and R. Main [from (*17*)]. We processed these to generate GRF traces of emus at a variety of speeds (see Supplementary Text for details), and the data from (*55*) also provided extra data points for DF and $\widehat{L}$.

The phase angle of the COM oscillations (ϕ_{COM}; in degrees) was calculated using a method similar to (*5*): We split up total COM energy into contributions due to horizontal and vertical velocity fluctuations of the COM and summed the vertical fluctuations with the gravitational potential energy of the COM. We computed the cross-correlation between these two contributors to total COM energy. ϕ_{COM} corresponded to the time shift at which the cross-correlation was maximal. We do not report the absolute phase angles but define ϕ_{COM} with respect to the vertical fluctuations (e.g., if $\phi_{\text{COM}} = 90°$, then the horizontal peak comes a quarter period after the vertical peak). For the purposes of our analysis, we operationalize grounded running as a gait that where ϕ_{COM} is less than 10° combined with a DF that is 0.5 or higher.

Supplementary Materials

The PDF file includes:

Other Supplementary Material for this manuscript includes the following:

REFERENCES AND NOTES

1. R. M. Alexander, *Principles of Animal Locomotion* (Princeton Univ. Press, 2006).
2. D. F. Hoyt, R. Taylor, Gait and the energetics of locomotion in horses. *Nature* **292**, 239–240 (1981).
3. C. R. Taylor, N. C. Heglund, G. M. O. Maloiy, Energetics and mechanics of terrestrial locomotion. I. Metabolic energy consumption as a function of speed and body size in birds and mammals. *J. Exp. Biol.* **97**, 1–21 (1982).
4. R. Kram, C. R. Taylor, Energetics of running: A new perspective. *Nature* **346**, 265–267 (1990).
5. J. Rubenson, D. B. Heliams, D. G. Lloyd, P. A. Fournier, Gait selection in the ostrich: Mechanical and metabolic characteristics of walking and running with and without an aerial phase. *Proc. R. Soc. Lond. B Biol. Sci.* **271**, 1091–1099 (2004).
6. R. R. Watson, J. Rubenson, L. Coder, D. F. Hoyt, M. W. G. Propert, R. L. Marsh, Gait-specific energetics contributes to economical walking and running in emus and ostriches. *Proc. R. Soc. B Biol. Sci.* **278**, 2040–2046 (2011).
7. G. A. Cavagna, N. C. Heglund, C. R. Taylor, Mechanical work in terrestrial locomotion: Two basic mechanisms for minimizing energy expenditure. *Am. J. Physiol.-Regul. Integr. Comp. Physiol.* **233**, R243–R261 (1977).
8. A. A. Biewener, Patterns of mechanical energy change in tetrapod gait: Pendula, springs and work. *J. Exp. Zoolog. A Comp. Exp. Biol* **305**, 899–911 (2006).
9. M. A. Daley, A. A. Biewener, Muscle force-length dynamics during level versus incline locomotion: A comparison of in vivo performance of two guinea fowl ankle extensors. *J. Exp. Biol.* **206**, 2941–2958 (2003).
10. T. J. Burkholder, R. L. Lieber, Sarcomere length operating range of vertebrate muscles during movement. *J. Exp. Biol.* **204**, 1529–1536 (2001).
11. K. A. McDonald, J. P. Cusumano, A. Hieronymi, J. Rubenson, Humans trade off whole-body energy cost to avoid overburdening muscles while walking. *Proc. R. Soc. B Biol. Sci.* **289**, 20221189 (2022).
12. D. T. Polet, The Murphy number: How pitch moment of inertia dictates quadrupedal walking and running energetics. *J. Exp. Biol.* **224**, jeb228296 (2021).
13. M. A. Daley, A. Birn-Jeffery, Scaling of avian bipedal locomotion reveals independent effects of body mass and leg posture on gait. *J. Exp. Biol.* **221**, jeb152538 (2018).
14. A. V. Birn-Jeffery, C. M. Hubicki, Y. Blum, D. Renjewski, J. W. Hurst, M. A. Daley, Don't break a leg: Running birds from quail to ostrich prioritise leg safety and economy on uneven terrain. *J. Exp. Biol.* **217**, 3786–3796 (2014).
15. A. A. Biewener, Biomechanics of mammalian terrestrial locomotion. *Science* **250**, 1097–1103 (1990).
16. C. T. Farley, C. R. Taylor, A mechanical trigger for the trot-gallop transition in horses. *Science* **253**, 306–308 (1991).
17. R. P. Main, A. A. Biewener, Skeletal strain patterns and growth in the emu hindlimb during ontogeny. *J. Exp. Biol.* **210**, 2676–2690 (2007).
18. M. M. Gilbert, E. Snively, J. Cotton, The tarsometatarsus of the ostrich *Struthio camelus*: Anatomy, bone densities, and structural mechanics. *PLOS ONE* **11**, e0149708 (2016).
19. R. M. N. Alexander, G. M. O. Maloiy, R. Njau, A. S. Jayes, Mechanics of running of the ostrich (*Struthio camelus*). *J. Zool.* **187**, 169–178 (1979).
20. A. E. Patak, J. Baldwin, Pelvic limb musculature in the emu *Dromaius novaehollandiae* (Aves: Struthioniformes: Dromaiidae): Adaptations to high-speed running. *J. Morphol.* **238**, 23–37 (1998).
21. M. A. Daley, A. J. Channon, G. S. Nolan, J. Hall, Preferred gait and walk–run transition speeds in ostriches measured using GPS-IMU sensors. *J. Exp. Biol.* **219**, 3301–3308 (2016).
22. A. E. Patak, "Anatomical and metabolic adaptations to locomotion in the emu (*Dromaius novaehollandiae* (Latham)), a giant flightless bird," PhD-thesis, Monash University, Melbourne (1988).
23. M. Eastman, *The Life of the Emu* (Angus & Robertson, 1969).
24. M. Ackermann, A. J. van den Bogert, Optimality principles for model-based prediction of human gait. *J. Biomech.* **43**, 1055–1060 (2010).
25. M. Srinivasan, Fifteen observations on the structure of energy-minimizing gaits in many simple biped models. *J. R. Soc. Interface* **8**, 74–98 (2011).
26. A. D. Kuo, The six determinants of gait and the inverted pendulum analogy: A dynamic walking perspective. *Hum. Mov. Sci.* **26**, 617–656 (2007).
27. T. A. McMahon, G. Valiant, E. C. Frederick, Groucho running. *J. Appl. Physiol.* **62**, 2326–2337 (1987).
28. S. M. Gatesy, A. A. Biewener, Bipedal locomotion: Effects of speed, size and limb posture in birds and humans. *J. Zool.* **224**, 127–147 (1991).
29. P. J. Bishop, D. F. Graham, L. P. Lamas, J. R. Hutchinson, J. Rubenson, J. A. Hancock, R. S. Wilson, S. A. Hocknull, R. S. Barrett, D. G. Lloyd, C. J. Clemente, The influence of speed

and size on avian terrestrial locomotor biomechanics: Predicting locomotion in extinct theropod dinosaurs. *PLOS ONE* **13**, e0192172 (2018).

30. A. Abourachid, S. Renous, Bipedal locomotion in ratites (Paleognatiform): Examples of cursorial birds. *Ibis* **142**, 538–549 (2000).

31. J. A. Hancock, N. J. Stevens, A. R. Biknevicius, Whole-body mechanics and kinematics of terrestrial locomotion in the elegant-crested tinamou *Eudromia elegans*. *Ibis* **149**, 605–614 (2007).

32. R. L. Nudds, L. P. Folkow, J. J. Lees, P. G. Tickle, K.-A. Stokkan, J. R. Codd, Evidence for energy savings from aerial running in the Svalbard rock ptarmigan (*Lagopus muta hyperborea*). *Proc. R. Soc. B Biol. Sci.* **278**, 2654–2661 (2011).

33. S. Davis, A. Fox, J. Bonacci, F. Davis, Mechanics, energetics and implementation of grounded running technique: A narrative review. *BMJ Open Sport Exerc. Med.* **6**, e000963 (2020).

34. E. Andrada, R. Blickhan, N. Ogihara, C. Rode, Low leg compliance permits grounded running at speeds where the inverted pendulum model gets airborne. *J. Theor. Biol.* **494**, 110227 (2020).

35. M. A. Daley, J. R. Usherwood, Two explanations for the compliant running paradox: Reduced work of bouncing viscera and increased stability in uneven terrain. *Biol. Lett.* **6**, 418–421 (2010).

36. N. C. Smith, A. M. Wilson, K. J. Jespers, R. C. Payne, Muscle architecture and functional anatomy of the pelvic limb of the ostrich (*Struthio camelus*). *J. Anat.* **209**, 765–779 (2006).

37. L. P. Lamas, R. P. Main, J. R. Hutchinson, Ontogenetic scaling patterns and functional anatomy of the pelvic limb musculature in emus (*Dromaius novaehollandiae*). *PeerJ* **2**, e716 (2014).

38. J. Rubenson, D. G. Lloyd, D. B. Heliams, T. F. Besier, P. A. Fournier, Adaptations for economical bipedal running: The effect of limb structure on three-dimensional joint mechanics. *J. R. Soc. Interface* **8**, 740–755 (2011).

39. T. J. Roberts, R. L. Marsh, P. G. Weyand, C. R. Taylor, Muscular force in running turkeys: The economy of minimizing work. *Science* **275**, 1113–1115 (1997).

40. A. Abourachid, C. Chevallereau, I. Pelletan, P. Wenger, An upright life, the postural stability of birds: A tensegrity system. *J. R. Soc. Interface* **20**, 20230433 (2023).

41. S. M. Cox, K. L. Easton, M. C. Lear, R. L. Marsh, S. L. Delp, J. Rubenson, The interaction of compliance and activation on the force-length operating range and force generating capacity of skeletal muscle: A computational study using a guinea fowl musculoskeletal model. *Integr. Org. Biol.* **1**, obz022 (2019).

42. K. Meijer, P. Bosch, M. F. Bobbert, A. J. van Soest, P. A. Huijing, The isometric knee extension moment-angle relationship: Experimental data and predictions based on cadaver data. *J. Appl. Biomech.* **14**, 62–79 (1998).

43. P. J. Bishop, K. B. Michel, A. Falisse, A. R. Cuff, V. R. Allen, F. De Groote, J. R. Hutchinson, Computational modelling of muscle fibre operating ranges in the hindlimb of a small ground bird (*Eudromia elegans*), with implications for modelling locomotion in extinct species. *PLOS Comput. Biol.* **17**, e1008843 (2021).

44. S. Macaulay, T. Hoehfurtner, S. R. R. Cross, R. D. Marek, J. R. Hutchinson, E. R. Schachner, A. E. Maher, K. T. Bates, Decoupling body shape and mass distribution in birds and their dinosaurian ancestors. *Nat. Commun.* **14**, 1575 (2023).

45. E. Andrada, J. A. Nyakatura, F. Bergmann, R. Blickhan, Adjustments of global and hindlimb local properties during the terrestrial locomotion of the common quail (*Coturnix coturnix*). *J. Exp. Biol.* **216**, jeb085399 (2013).

46. J. R. Rebula, A. D. Kuo, The cost of leg forces in bipedal locomotion: A simple optimization study. *PLOS ONE* **10**, e0117384 (2015).

47. D. T. Polet, J. E. A. Bertram, An inelastic quadrupedal model discovers four-beat walking, two-beat running, and pseudo-elastic actuation as energetically optimal. *PLOS Comput. Biol.* **15**, e1007444 (2019).

48. A. Falisse, G. Serrancolí, C. L. Dembia, J. Gillis, I. Jonkers, F. De Groote, Rapid predictive simulations with complex musculoskeletal models suggest that diverse healthy and pathological human gaits can emerge from similar control strategies. *J. R. Soc. Interface* **16**, 20190402 (2019).

49. G. Serrancoli, A. Falisse, C. Dembia, J. Vantilt, K. Tanghe, D. Lefeber, I. Jonkers, J. De Schutter, F. De Groote, Subject-exoskeleton contact model calibration leads to accurate interaction force predictions. *IEEE Trans. Neural Syst. Rehabil. Eng.* **27**, 1597–1605 (2019).

50. R. H. Miller, B. R. Umberger, J. Hamill, G. E. Caldwell, Evaluation of the minimum energy hypothesis and other potential optimality criteria for human running. *Proc. R. Soc. B Biol. Sci.* **279**, 1498–1505 (2012).

51. A. D. Koelewijn, E. Dorschky, A. J. van den Bogert, A metabolic energy expenditure model with a continuous first derivative and its application to predictive simulations of gait. *Comput. Methods Biomech. Biomed. Engin.* **21**, 521–531 (2018).

52. F. De Groote, A. L. Kinney, A. V. Rao, B. J. Fregly, Evaluation of direct collocation optimal control problem formulations for solving the muscle redundancy problem. *Ann. Biomed. Eng.* **44**, 2922–2936 (2016).

53. N. Haralabidis, G. Serrancolí, S. Colyer, I. Bezodis, A. Salo, D. Cazzola, Three-dimensional data-tracking simulations of sprinting using a direct collocation optimal control approach. *PeerJ* **9**, e10975 (2021).

54. W. I. Sellers, P. L. Manning, Estimating dinosaur maximum running speeds using evolutionary robotics. *Proc. R. Soc. B Biol. Sci.* **274**, 2711–2716 (2007).

55. J. E. Goetz, T. R. Derrick, D. R. Pedersen, D. A. Robinson, M. G. Conzemius, T. E. Baer, T. D. Brown, Hip joint contact force in the emu (*Dromaius novaehollandiae*) during normal level walking. *J. Biomech.* **41**, 770–778 (2008).

56. W. I. Sellers, L. Margetts, R. A. Coria, P. L. Manning, March of the titans: The locomotor capabilities of sauropod dinosaurs. *PLOS ONE* **8**, e78733 (2013).

57. J. R. Hutchinson, J. W. Rankin, J. Rubenson, K. H. Rosenbluth, R. A. Siston, S. L. Delp, Musculoskeletal modelling of an ostrich (*Struthio camelus*) pelvic limb: Influence of limb orientation on muscular capacity during locomotion. *PeerJ* **3**, e1001 (2015).

58. J. W. Rankin, J. Rubenson, J. R. Hutchinson, Inferring muscle functional roles of the ostrich pelvic limb during walking and running using computer optimization. *J. R. Soc. Interface* **13**, 20160035 (2016).

59. A. M. Luger, P. J. Watson, H. Dutel, M. J. Fagan, L. Van Hoorebeke, A. Herrel, D. Adriaens, Regional patterning in tail vertebral form and function in chameleons (*Chamaeleo calyptratus*). *Integr. Comp. Biol.* **61**, 455–463 (2021).

60. C. L. Dembia, N. A. Bianco, A. Falisse, J. L. Hicks, S. L. Delp, OpenSim Moco: Musculoskeletal optimal control. *PLOS Comput. Biol.* **16**, e1008493 (2020).

61. S. J. J. F. Davies, *Ratites and Tinamous*, Bird Families of the World (Oxford Univ. Press, 2002).

62. A. R. Cuff, M. A. Daley, K. B. Michel, V. R. Allen, L. P. Lamas, C. Adami, P. Monticelli, L. Pelligand, J. R. Hutchinson, Relating neuromuscular control to functional anatomy of limb muscles in extant archosaurs. *J. Morphol.* **280**, 666–680 (2019).

63. A. Patak, J. Baldwin, Structural and metabolic characterization of the muscles used to power running in the emu (*Dromaius novaehollandiae*), a giant flightless bird. *J. Exp. Biol.* **175**, 233–249 (1993).

64. A. Badri-Spröwitz, A. Aghamaleki Sarvestani, M. Sitti, M. A. Daley, BirdBot achieves energy-efficient gait with minimal control using avian-inspired leg clutching. *Sci. Robot.* **7**, eabg4055 (2022).

65. T. J. Roberts, R. Kram, P. G. Weyand, C. R. Taylor, Energetics of bipedal running: I. Metabolic cost of generating force. *J. Exp. Biol.* **201**, 2745–2751 (1998).

66. A. Ruina, J. E. A. Bertram, M. Srinivasan, A collisional model of the energetic cost of support work qualitatively explains leg sequencing in walking and galloping, pseudo-elastic leg behavior in running and the walk-to-run transition. *J. Theor. Biol.* **237**, 170–192 (2005).

67. J. Doke, J. M. Donelan, A. D. Kuo, Mechanics and energetics of swinging the human leg. *J. Exp. Biol.* **208**, 439–445 (2005).

68. F. K. Fuss, Tibiofibular junction of the South African ostrich (*Struthio camelus australis*). *J. Morphol.* **227**, 213–226 (1996).

69. M. J. Schwaner, J. C. Gordon, A. A. Biewener, M. A. Daley, Muscle force–length dynamics during walking over obstacles indicates delayed recovery and a shift towards more 'strut-like' function in birds with proprioceptive deficit. *J. Exp. Biol.* **226**, jeb245199 (2023).

70. B. Grossi, J. Iriarte-Díaz, O. Larach, M. Canals, R. A. Vásquez, Walking like dinosaurs: Chickens with artificial tails provide clues about non-avian theropod locomotion. *PLOS ONE* **9**, e88458 (2014).

71. N. U. Schaller, B. Herkner, R. Villa, P. Aerts, The intertarsal joint of the ostrich (*Struthio camelus*): Anatomical examination and function of passive structures in locomotion. *J. Anat.* **214**, 830–847 (2009).

72. Y.-H. Chang, L. H. Ting, Mechanical evidence that flamingos can support their body on one leg with little active muscular force. *Biol. Lett.* **13**, 20160948 (2017).

73. C. J. Clemente, P. J. Bishop, N. Newman, S. A. Hocknull, Steady bipedal locomotion with a forward situated whole-body centre of mass: The potential importance of temporally asymmetric ground reaction forces. *J. Zool.* **304**, 193–201 (2018).

74. M. T. Carrano, A. A. Biewener, Experimental alteration of limb posture in the chicken (*Gallus gallus*) and its bearing on the use of birds as analogs for dinosaur locomotion. *J. Morphol.* **240**, 237–249 (1999).

75. J. R. Usherwood, T. Y. Hubel, B. J. H. Smith, Z. T. Self Davies, G. Sobota, The scaling or ontogeny of human gait kinetics and walk-run transition: The implications of work vs. peak power minimization. *J. Biomech.* **81**, 12–21 (2018).

76. S. J. Portugal, C. P. Murn, E. L. Sparkes, M. A. Daley, The fast and forceful kicking strike of the secretary bird. *Curr. Biol.* **26**, R58–R59 (2016).

77. W. I. Sellers, S. B. Pond, C. A. Brassey, P. L. Manning, K. T. Bates, Investigating the running abilities of *Tyrannosaurus rex* using stress-constrained multibody dynamic analysis. *PeerJ* **5**, e3420–e3419 (2017).

78. S. M. Gatesy, Caudofemoral musculature and the evolution of theropod locomotion. *Paleobiology* **16**, 170–186 (1990).

79. P. A. van Bijlert, A. J. "K." van Soest, A. S. Schulp, Natural frequency method: Estimating the preferred walking speed of *Tyrannosaurus rex* based on tail natural frequency. *R. Soc. Open Sci.* **8**, rsos.201441 (2021).

80. J. R. Hutchinson, V. Ng-Thow-Hing, F. C. Anderson, A 3D interactive method for estimating body segmental parameters in animals: Application to the turning and running performance of *Tyrannosaurus rex*. *J. Theor. Biol.* **246**, 660–680 (2007).

81. P. J. Bishop, C. J. Clemente, R. E. Weems, D. F. Graham, L. P. Lamas, J. R. Hutchinson, J. Rubenson, R. S. Wilson, S. A. Hocknull, R. S. Barrett, D. G. Lloyd, Using step width to compare locomotor biomechanics between extinct, non-avian theropod dinosaurs and modern obligate bipeds. *J. R. Soc. Interface* **14**, 20170276 (2017).

82. L. Ren, J. R. Hutchinson, The three-dimensional locomotor dynamics of African (*Loxodonta africana*) and Asian (*Elephas maximus*) elephants reveal a smooth gait transition at moderate speed. *J. R. Soc. Interface* **5**, 195–211 (2008).

83. J. J. Genin, P. A. Willems, G. A. Cavagna, R. Lair, N. C. Heglund, Biomechanics of locomotion in Asian elephants. *J. Exp. Biol.* **213**, 694–706 (2010).

84. K. T. Bates, L. Wang, M. Dempsey, S. Broyde, M. J. Fagan, P. G. Cox, Back to the bones: Do muscle area assessment techniques predict functional evolution across a macroevolutionary radiation? *J. R. Soc. Interface* **18**, 20210324 (2021).

85. E. Andrada, J. Nyakatura, R. Müller, C. Rode, R. Blickhan, "Grounded running: An overlooked strategy for robots" in *Autonomous Mobile Systems 2012*, P. Levi, O. Zweigle, K. Häußermann, B. Eckstein, Eds., Informatik Aktuell (Springer, 2012), pp. 79–87.

86. J. Rubenson, D. G. Lloyd, T. F. Besier, D. B. Heliams, P. A. Fournier, Running in ostriches (*Struthio camelus*): Three-dimensional joint axes alignment and joint kinematics. *J. Exp. Biol.* **210**, 2548–2562 (2007).

87. S. S. Blemker, S. L. Delp, Rectus femoris and vastus intermedius fiber excursions predicted by three-dimensional muscle models. *J. Biomech.* **39**, 1383–1391 (2006).

88. L. J. Bhargava, M. G. Pandy, F. C. Anderson, A phenomenological model for estimating metabolic energy consumption in muscle contraction. *J. Biomech.* **37**, 81–88 (2004).

89. S. K. Maloney, T. J. Dawson, Sexual dimorphism in basal metabolism and body temperature of a large bird, the emu. *The Condor* **95**, 1034–1037 (1993).

90. K. K. Lemaire, R. T. Jaspers, D. A. Kistemaker, A. J. "K." van Soest, W. J. van der Laarse, Metabolic cost of activation and mechanical efficiency of mouse soleus muscle fiber bundles during repetitive concentric and eccentric contractions. *Front. Physiol* **10**, 760 (2019).

91. J. Vanden Berge, G. A. Zweers, "Myologia" in *Handbook of Avian Anatomy: Nomina Anatomica Avium*, J. J. Baumel, A. S. King, J. E. Breazile, H. E. Evans, J. Vanden Berge, Eds. (Publications of the Nuttall Ornithological Club, ed. 2, 1993), pp. 189–247.

92. A. V. Hill, The heat of shortening and the dynamic constants of muscle. *Proc. R. Soc. B Biol. Sci.* **126**, 136–195 (1938).

93. F. E. Zajac, Muscle and tendon: Properties, models, scaling and application to biomechanics and motor control. *Crit. Rev. Biomed. Eng.* **17**, 359–411 (1989).

94. A. Seth, J. L. Hicks, T. K. Uchida, A. Habib, C. L. Dembia, J. J. Dunne, C. F. Ong, M. S. DeMers, A. Rajagopal, M. Millard, S. R. Hamner, E. M. Arnold, J. R. Yong, S. K. Lakshmikanth, M. A. Sherman, J. P. Ku, S. L. Delp, OpenSim: Simulating musculoskeletal dynamics and neuromuscular control to study human and animal movement. *PLOS Comput. Biol.* **14**, e1006223 (2018).

95. F. E. Nelson, A. M. Gabaldón, T. J. Roberts, Force–velocity properties of two avian hindlimb muscles. *Comp. Biochem. Physiol. A Mol. Integr. Physiol.* **137**, 711–721 (2004).

96. R. M. Enoka, J. Duchateau, Translating fatigue to human performance. *Med. Sci. Sports Exerc.* **48**, 2228–2238 (2016).

97. M. A. Sherman, A. Seth, S. L. Delp, Simbody: Multibody dynamics for biomedical research. *Procedia IUTAM* **2**, 241–261 (2011).

98. L. P. Lamas, "Musculoskeletal biomechanics during growth on emu (Dromaius; Aves): An integrative experimental and modelling analysis," PhD-thesis, Royal Veterinary College, London (2015).

99. D. Gangl, G. E. Weissengruber, M. Egerbacher, G. Forstenpointner, Anatomical description of the muscles of the pelvic limb in the ostrich (*Struthio camelus*). *Anat. Histol. Embryol. J. Vet. Med. Ser. C* **33**, 100–114 (2004).

100. A. V. Zinoviev, Notes on the hind limb myology of the ostrich (*Struthio camelus*). *Ornithologia* **33**, 53–62 (2006).